Published in final edited form as:
Neuron. 2010 December 22; 68(6): 1067–1081. doi:10.1016/j.neuron.2010.11.030.

Tau mislocalization to dendritic spines mediates synaptic dysfunction independently of neurodegeneration

Brian R. Hoover[1,3,#], **Miranda N. Reed**[1,3,#], **Jianjun Su**[2], **Rachel D. Penrod**[2], **Linda A. Kotilinek**[1,3], **Marianne K. Grant**[1,3], **Rose Pitstick**[4], **George A. Carlson**[4], **Lorene M. Lanier**[2], **Li-Lian Yuan**[2,3], **Karen H. Ashe**[1,2,3,5,*], and **Dezhi Liao**[2,3,*]

[1]Department of Neurology, University of Minnesota, Minneapolis, MN 55455

[2]Department of Neuroscience, University of Minnesota, Minneapolis, MN 55455

[3]N. Bud Grossman Center for Memory Research and Care, University of Minnesota, Minneapolis, MN 55455

[4]McLaughlin Research Institute, Great Falls, MT 59405

[5]Geriatric Research Education and Clinical Center and the Veterans Administration Medical Center, Minneapolis, MN 55417

Abstract

The microtubule-associated protein tau accumulates in Alzheimer's and other fatal dementias, which manifest when forebrain neurons die. Recent advances in understanding these disorders indicate that brain dysfunction precedes neurodegeneration, but the role of tau is unclear. Here, we show that early tau-related deficits develop not from the loss of synapses or neurons, but rather as a result of synaptic abnormalities caused by the accumulation of hyperphosphorylated tau within intact dendritic spines, where it disrupts synaptic function by impairing glutamate receptor trafficking or synaptic anchoring. Mutagenesis of 14 disease-associated serine and threonine amino acid residues to create pseudohyperphosphorylated tau caused tau mislocalization while creation of phosphorylation-deficient tau blocked the mis-targeting of tau to dendritic spines. Thus, tau phosphorylation plays a critical role in mediating tau mislocalization and subsequent synaptic impairment. These data establish that the locus of early synaptic malfunction caused by tau resides in dendritic spines.

Introduction

Neurofibrillary tangles, the most common intraneuronal inclusion and a cardinal feature of Alzheimer's disease (AD), appear when tau forms insoluble aggregates (reviewed in Avila et al., 2004; Gendron and Petrucelli, 2009). Once believed to mediate neuronal death and cognitive deficits, observations in mouse models have since shown that tangles exert negligible neurotoxicity compared to soluble tau (SantaCruz et al., 2005; Oddo et al., 2006). However, it is unclear how soluble tau disrupts brain function. Healthy neurons maintain a spatial gradient of tau, whose concentration is greater in axons than in somatodendritic

[*]To whom correspondence should be addressed: liaox020@umn.edu or hsiao005@umn.edu .
[#]These authors contributed equally to this work.

compartments (Papasozomenos and Binder, 1987; for review, see Buee et al., 2000; Avila et al., 2004). In neurological disorders, such as AD, the gradient becomes inverted (reviewed in Buee et al., 2000; Brandt et al., 2005; Gendron and Petrucelli, 2009), potentially disrupting kinesin and dynein motor protein function and axonal transport (Mandelkow et al., 2003; Dixit et al., 2008), permitting direct neurotoxic interactions between tau and the actin cytoskeleton (Fulga et al., 2007), or enabling the accumulation of tau aggregates in the dendrites of neurons damaged by severe axonal and synapse loss (Yoshiyama et al., 2007). These hypotheses may explain how tau induces neurodegeneration, which correlates well with symptoms (reviewed in Buee et al., 2000; Avila et al., 2004; Brandt et al., 2005), but do not address how tau diminishes brain function at the preclinical stages of disease immediately preceding neurodegeneration (Arvanitakis et al., 2007; Petrie et al., 2009). We investigated how tau induces early memory deficits and disrupts synaptic plasticity, prior to overt synaptic or neuronal degeneration, using both *in vivo* and *in vitro* models.

Results

Cognitive impairments and htau mislocalization in rTgP301L mice

In the rTg4510 mouse model of tauopathy, which exhibits the regulated expression of P301L human tau (htau) associated with frontotemporal dementia with Parkinsonism linked to chromosome 17 (FTDP-17), called rTgP301L here, we focused our initial investigations upon mice at 1.3 and 4.5 months of age, prior to the loss of synapses or neurons (Ramsden et al., 2005; SantaCruz et al., 2005), and found spatial memory deficits first appearing in the older mice (Figure 1). Examination of spatial reference memory with the Morris water maze (Westerman et al., 2002) demonstrated cognitive impairments in 4.5, but not 1.3, month-old rTgP301L mice (*$p < 0.05$ by repeated-measures ANOVA; Figures 1A–1C). We found a direct correspondence between deficits in spatial reference memory and impaired long-lasting synaptic plasticity in the hippocampus. Specifically, long-term potentiation (LTP) in the CA1 hippocampal region was only impaired in 4.5-month old rTgP301L mice (*$p < 0.05$ by repeated-measures ANOVA; Figures 1D and 1E), which suggested the possibility of postsynaptic abnormalities. Taken together with the observation that htau interacts directly with filamentous (F) actin (Fulga et al., 2007; He et al., 2009), which concentrates in dendritic spines to a much greater degree than in dendritic shafts (Fifkova and Delay, 1982; Hering and Sheng, 2001), we tested the idea that in rTgP301L mice htau mislocalizes to dendritic spines, the fundamental postsynaptic units for information processing and memory storage in the mammalian brain (Hering and Sheng, 2001). To control for the possible effects of htau overexpression, we created rTg21221 mice, termed rTgWT here, expressing wildtype (WT) htau at concentrations equivalent to P301L htau in rTgP301L mice. Unlike rTgP301L mice, rTgWT mice show neither progressive memory deficits nor neurodegeneration (**$p < 0.01$, ***$p < 0.001$, ****$p < 0.0001$ by repeated-measures ANOVA and ANOVA; Figures 2 and S1). We prepared isolates from forebrain lysates of 4.5-month old rTgP301L, rTgWT and transgenic negative (TgNeg) mice enriched in both pre- and postsynaptic proteins, termed the S2 fraction, and in postsynaptic density proteins, termed PSD-1 (Figure 3). We found equivalent levels of htau in the S2 fractions of both transgenic mouse lines (Figures 3A and 3C), but significantly higher htau levels in PSD-1 preparations from rTgP301L mice (*$p < 0.05$ by t-test; Figures 3B and 3D). The lack of differences in PSD95 levels in PSD-1 preparations from TgNeg, rTgWT and rTgP301L mice ($p = 0.95$ by ANOVA; Figure 3E) indicated that the dendritic spines in rTgP301L mice remained largely intact, despite the impairments of memory and synaptic plasticity. As an additional control measure, we confirmed that PSD95 levels did not change in relation to α-tubulin ($p = 0.76$ by ANOVA; Figure 3F). The association of abnormalities in memory and synaptic plasticity with the presence of htau in dendritic spines led us to hypothesize that

htau mislocalization to spines is an early pathological process that disrupts synaptic function. We tested this hypothesis *in vitro* using cultured rat and mouse neurons.

P301L htau is aberrantly localized to dendritic spines

To visualize the cellular distribution of WT and P301L htau, we transfected dissociated rat hippocampal neurons with plasmids encoding GFP alone, or co-transfected with plasmids encoding DsRed protein and GFP-tagged htau, at 7–10 days in vitro (DIV) and photographed the neurons two weeks later (Figures 4A, 4B and S2). We found GFP-tagged htau in both axons and dendrites (Figures 4A and 4B), in keeping with immunohistochemical studies in monkey brain (Papasozomenos and Binder, 1987). Neurons expressing GFP alone and GFP-tagged htau showed equivalent spine densities, consistent with observations in transfected organotypic hippocampal slice cultures expressing htau (Shahani et al., 2006) ($p = 0.83$ by ANOVA; black bars in Figure 4C). Importantly, although WT htau rarely localized to DsRed-labeled dendritic spines, P301L htau appeared in the majority of the spines (Figures 4A and 4B). While the total number of DsRed-labeled dendritic spines ("all spines") was significantly higher than tau-containing spines ("spines with tau") in neurons expressing WT or P301L htau (Figure 4C), significantly more spines contained P301L than WT htau (***$p < 0.001$ by Bonferroni post-hoc analysis; 31 ± 3 P301L htau-containing spines out of 42 ± 3 total spines vs 8 ± 2 WT htau-containing spines out of 43 ± 4 total spines; Figure 4C), and the proportion of tau-containing spines was significantly higher in neurons expressing P301L htau (***$p < 0.001$ by t-test; 75 ± 3% for P301L vs 23 ± 5% for WT htau; Figure 4D). These *in vitro* data corroborated our biochemical analyses of WT and P301L htau in postsynaptic protein complexes *in vivo* (see Figure 3). Neither our *in vivo* nor *in vitro* experiments examined the potential interactions between htau and rodent tau.

Mislocalized htau impairs synaptic function

To determine whether mislocalized htau affected dendritic spine function, we recorded miniature excitatory postsynaptic currents (mEPSCs) in mature (22–30 DIV) rat hippocampal neurons expressing GFP alone or GFP-tagged htau (Figure 4E). The majority of presynaptic inputs originated from untransfected neurons, since virtually no GFP-fluorescent axons innervated transfected neurons due to the minute proportion (<10%) of neurons transfected with GFP-tagged htau. We thus attributed any changes in mEPSCs to the modulation of postsynaptic activities by the htau in spines. Large mEPSCs (amplitude >20 pA; see arrows in Figures 4E1 and 4E2) occurred more frequently in neurons expressing GFP or WT htau than in neurons expressing P301L htau (***$p < 0.001$ by Kolmogorov-Smirnov analysis for P301L vs GFP; Figures 4E3 and 4F). P301L, but not WT, htau significantly reduced the mean amplitude (***$p < 0.001$ by Fisher's PLSD post-hoc analysis; Figure 4G) and frequency of mEPSCs (***$p < 0.001$ by Fisher's PLSD post-hoc analysis Figure 4G) compared to GFP-transfected neurons.

We found similar P301L htau-mediated changes in the amplitude (***$p < 0.001$ by Fisher's PLSD post-hoc analysis for P301L vs rTgWT and TgNeg) and frequency (*$p < 0.05$ by Fisher's PLSD post-hoc analysis for P301L vs rTgWT and TgNeg) of mEPSCs in neurons cultured from rTgP301L mice, compared to those cultured from rTgWT and TgNeg mice (Figures 5A–5C). Because the P301L htau-mediated electrophysiological changes in mouse neurons mimicked the effects seen in htau-expressing rat neurons where the majority of presynaptic inputs originated from untransfected neurons, we attributed the changes in mEPSCs to the modulation of postsynaptic activities by the htau in spines, suggesting that axonal tau contributed minimally to the synaptic deficits in our *in vitro* experimental system and indicating that P301L htau diminished synaptic function whether its expression originated from a genomic or an extragenomic cistron. However, our results cannot exclude

possible presynaptic roles of tau in the pathological development of neurodegenerative diseases. We noted that in both rat and mouse neurons, the expression of WT htau caused a small but significant decrease (*$p < 0.05$ by Kolmogorov-Smirnov analysis for WT vs GFP [Figure 4F] or WT vs TgNeg [Figure 5B]) in the probability of large mEPSC events (Figure 4F for rat and Figure 5B for mouse), suggesting that WT htau can also impair synaptic function. Presumably, this is related to the small amount of WT htau in spines (Figures 3B, 3D, 4C and 4D).

Impaired synaptic function is associated with decreased synaptic expression of AMPA and NMDA receptors with no visible loss of spines

The reduced amplitude of mEPSCs caused by P301L htau suggests a reduction in the amount of functional AMPA receptors (AMPARs) on the postsynaptic membrane, which has been proposed to be a common mechanism underlying reductions in synaptic strength (Malinow and Malenka, 2002; Newpher and Ehlers, 2008). The reduced frequency of mEPSCs, in the absence of spine loss (Figures 3E and 4C), suggests either an increase in the number of “silent synapses” or undetected weak synapses due to loss of synaptic AMPARs (Liao et al., 1995; Isaac et al., 1995). Therefore, we measured synaptic AMPARs. We labeled surface AMPARs in living neurons cultured from TgNeg, rTgWT and rTgP301L mice using a rabbit antibody against the N-terminus of glutamate receptor (GluR) type 1 subunits (N-GluR1) and labeled dendritic spines using a mouse antibody against PSD95 (Figure 5D). We found distinct clusters of AMPARs co-localizing with PSD95 in both TgNeg and rTgWT neurons (denoted by arrows in upper panels in Figure 5D), but not in rTgP301L neurons, in which weak N-GluR1 immunoreactivity appeared along the dendritic shafts as diffuse staining rather than distinct clusters (see triangles in the lower panels in Figure 5D). Importantly, despite a significant reduction in the fluorescence intensity of N-GluR1 co-localizing with PSD95 immunoreactivity in spines of rTgP301L neurons (***$p < 0.001$ by Fisher’s PLSD post-hoc analysis; Figure 5E), the total number of PSD95 clusters remained unchanged (Figure 5F), indicating that the impairment of synaptic function caused by the accumulation of htau in spines occurred without the overt loss of postsynaptic structures. Since the stability and existence of dendritic spines can be compromised by the prolonged absence of functional synaptic AMPARs (McKinney et al., 1999; Richards et al., 2005; McKinney, 2010), the loss of AMPARs reported here might be a cellular alteration that leads to the previous observation that dendritic spines degenerate in AD and in older mice modeling tauopathies, including rTgP301L and P301S (Davies et al., 1987; Selkoe, 2002; Hsieh et al., 2006; Eckermann et al., 2007; Yoshiyama et al., 2007; Smith et al., 2009; Rocher et al., 2010; for review, see Knobloch and Mansuy, 2008).

To determine whether the decreased expression of synaptic GluR1 in rTgP301L neurons reflects a widespread tau-mediated inhibitory effect on synaptic glutamate receptor expression, we also examined levels of intracellular and synaptic GluR1, GluR2/3 and NMDA receptor (NMDAR) subunit 1A (NR1) in fixed mouse cultures prepared from TgNeg, rTgWT and rTgP301L mice (Figure 6). Immunocytochemical detection of glutamate receptors in fixed neurons provides a snapshot of receptor cluster localization at the time of fixation. We labeled total GluR1 and 2/3 receptors in fixed neurons cultured from TgNeg, rTgWT and rTgP301L mice using two different rabbit polyclonal antibodies against the C-terminus of GluR1 or GluR2/3 subunits (Liao et al., 1999) and labeled dendritic spines using a mouse antibody against PSD95 (Figures 6A, 6B). We found distinct clusters of GluRs co-localizing with PSD95 in both TgNeg and rTgWT neurons (denoted by small arrows in the upper panels of Figures 6A, 6B), but not in rTgP301L neurons, in which weak GluR immunoreactivity appeared along the dendritic shafts as diffuse staining rather than distinct clusters (see large arrows in the lower panels of Figures 6A, 6B). Normalization of GluR1 and GluR2/3 fluorescence intensity in spines to their respective

fluorescence intensity in dendritic shafts demonstrated that the synaptic expression of GluR1 and GluR2/3 receptors are decreased in rTgP301L mice compared to TgNeg (***$p < 0.001$ by Fisher's PLSD post-hoc analysis; Figure 6D) and rTgWT neurons (*$p < 0.05$ and **$p < 0.01$ by Fisher's PLSD post-hoc analysis; Figure 6D). As reported previously, (Liao et al., 1999), synaptic GluR1 receptor expression detected on fixed neurons (Figure 6A) strongly corresponded to surface N-GluR1 receptor expression detected on living neurons (Figure 5D). Labeling of total NR1 receptors with a rabbit polyclonal antibody against the N-terminus of NR1 (Liao et al., 1999) in fixed neurons cultured from these three lines of mice revealed a similar pattern of expression (Figure 6C). In TgNeg and rTgWT neurons, NR1 receptors are clustered in spines as identified by the strong overlap between PSD95 and NR1 expression (small arrows in upper panels of Figure 6C). In contrast, the large arrows in the lower panels of Figure 6C indicate the reduced colocalization of PSD95 and NR1 in rTgP301L neurons. Normalization of NR1 fluorescence intensity in spines to that in the dendritic shafts demonstrated that the synaptic expression of NR1 receptors are decreased in rTgP301L mice compared to TgNeg and rTgWT neurons (***$p < 0.001$ by Fisher's PLSD post-hoc analysis; Figure 6D). Our results indicate that tau mislocalization to dendritic spines damages these spines profoundly by disrupting the synaptic targeting or anchoring of both AMPA and NMDA receptors.

Role of phosphorylation in htau mislocalization

We postulated that the mislocalization of tau in spines depends upon abnormal htau hyperphosphorylation, which occurs to a greater extent in rTgP301L than rTgWT mice (Figure 7). Tau consists of at least three structurally distinct regions, including an amino-terminal projection domain and a carboxyl-terminal domain that contains repetitive microtubule-binding motifs flanked by proline-rich regions (Buee et al., 2000;Avila et al., 2004). Hyperphosphorylation of htau at the 14 serine (S) and threonine (T) residues that can be phosphorylated by proline (P)-directed S/T kinases has been shown to modulate tau neurotoxicity, control tau binding to F-actin and regulate the effect of htau on the viability of retinal neurons in the fruit fly (Fulga et al., 2007;Steinhilb et al., 2007a,2007b). The neurons of fruit flies, like other lower organisms, lack dendritic spines (Hering and Sheng, 2001). Therefore, the relevance of this finding to mammalian neurons, where F-actin concentrates in dendritic spines, has not been established. To validate that P301L htau is hyperphosphorylated *in vitro* on SP/TP residues previously implicated in tau neurotoxicity, we examined htau phosphorylation levels in our rat neuron cultures expressing WT or P301L htau. Changes in tau phosphorylation underlying tau pathology have a temporally specific sequence (Maurage et al., 2003;Luna-Munoz et al., 2007;Bertrand et al., 2010) and two of the earliest changes in tau phosphorylation levels occur at phosphoepitopes S199 and T231 (Maurage et al., 2003;Luna-Munoz et al., 2007;Bertrand et al., 2010). We hypothesize that the P301L htau-mediated synaptic dysfunction is one of the earliest signs of tau pathology. Therefore, we compared the phosphorylation status of S199 and T231 in rat neurons expressing WT or P301L htau. Following immunoprecipitation and immunoblotting of htau from cell lysates prepared from WT or P301L htau-expressing rat neurons, we found significantly higher levels of phosphorylated S199 in neurons expressing P301L htau than in neurons expressing WT htau (Figures 8A, 8B). We also found a non-significant increase in phosphorylated T231 levels in cultures expressing P301L htau (data not shown). Alz-50, a marker of advanced changes in pathological conformation and phosphorylation states of tau could not be detected in neurons expressing WT or P301L htau (Figure 8A). Taken together, these results support our hypothesis that tau-mediated synaptic dysfunction is due, at least in part, to very early changes in tau phosphorylation. To ascertain further whether proline-directed phosphorylation controls the mislocalization of htau to the dendritic spines of mammalian neurons, we changed the 14 SP/TP residues in GFP-tagged WT and P301L htau either to nonpolar alanine residues to prevent phosphorylation, termed AP for alanine-

proline here, or to negatively charged glutamate residues to mimic phosphorylation, termed E14 here (Fulga et al., 2007;Steinhilb et al., 2007a). As in previous experiments, we measured htau in dendritic spines in rat neurons co-transfected with plasmids encoding DsRed and each of six different htau proteins (Figure 8C). AP htau and AP/P301L htau accumulated in spines significantly less than even WT htau (***$p < 0.001$ by Bonferroni post-hoc analysis; 5 ± 2%, AP/P301L: 1 ± 1%, WT: 23 ± 5%; Figure 8D). Conversely, E14 htau and E14/P301L htau localized to spines more frequently than WT htau (***$p < 0.001$ by Bonferroni post-hoc analysis; E14: 80 ± 3%, E14/P301L: 83 ± 3%, WT: 23 ± 5%; Figure 8D).

To ensure that each GFP-htau construct was expressed in individually transfected hippocampal neurons at an equivalent level in the primary neuronal cultures, GFP-positive neurons were separated from untransfected neurons by flow cytometry (Figure 9). The amount of GFP-tagged WT and mutant htau was quantified by measuring the fluorescence intensity levels of isolated GFP-positive cells in suspension. We found equivalent levels of mean GFP fluorescence intensity across all GFP-htau transfected neuron populations ($p = 0.44$ by ANOVA; Figures 9A, 9B). Although flow cytometry provides a measure of the expression levels of GFP-htau in the neuronal cell body and any processes that remained attached through the cell collection and dissociation procedure, this method does not selectively measure htau levels in dendritic shafts. To quantify GFP-htau expression in dendritic shafts, we measured fluorescence intensity in the dendritic shafts and found equivalent levels of htau in all six transfectants ($p = 0.91$ by ANOVA; Figure 9C). There were no significant differences in spine density among the different transfected neuronal cultures (data not shown; $p = 0.83$ by ANOVA). Taken together, these data indicate comparable levels of htau expression and no spine toxicity using all of the GFP-htau variants.

In electrophysiological studies, we confirmed our earlier observation that significant reductions in the amplitude (***$p < 0.001$ by Fisher's PLSD post-hoc analysis) and frequency (**$p < 0.01$ and ***$p < 0.001$ by Fisher's PLSD post-hoc analysis) of mEPSCs occur when htau has accumulated in the dendritic spines (Figures 10A–10D). Collectively, these results demonstrate that the mislocalization of tau in dendritic spines and subsequent synaptic dysfunction depend upon proline-directed phosphorylation of tau.

Discussion

Identification of the earliest neuronal dysfunction associated with tau-mediated pathologies preceding neurodegeneration is critical for understanding the pathophysiology of neurodegenerative diseases. An early pathological hallmark of tauopathies is the abnormal sorting of htau into the somatodendritic compartment of neurons where hyperphosphorylated htau aggregates (for review, see Avila et al., 2004; Gendron and Petrucelli, 2009). The physiological effects of this mis-sorting are unknown. Here, we demonstrated that htau is enriched in the PSD of rTgP301L mice compared to rTgWT mice. Likewise, in primary neurons expressing P301L or WT htau, mutant tau localized to dendritic spines more than WT htau does. Together, these results indicate that htau protein is not only mis-sorted into dendrites, but also into dendritic spines. The mis-sorted tau caused early synaptic dysfunction by suppressing AMPAR-mediated synaptic responses, probably through a global disruption of postsynaptic targeting or anchoring of glutamate receptors. Our findings confirm, complement and extend a recent study reporting that htau associates with the PSD complex, has a role in targeting fyn kinase to postsynaptic compartments and is involved in coupling NMDARs to PSD95 (Ittner et al., 2010). Our results go on to demonstrate, for the first time, the dependence of htau mislocalization to dendritic spines

upon htau hyperphosphorylation, and the deleterious effects that htau mislocalization exerts on both AMPARs and NMDARs (see model in Figure 10E).

The present study demonstrates that tau phosphorylation plays a critical role in tau mislocalization to dendritic spines. Phosphorylation is a well-known regulator of tau functions such as stabilizing microtubules and promoting their assembly and dynamic stability (reviewed in Avila et al., 2004; Gong et al., 2005). Here, we showed that the phosphorylation state of 14 disease-relevant S and T residues also critically regulates tau mislocalization to dendritic spines and the functional impairments that follow. Changes in the phosphorylation state of tau disrupt tau-microtubule interactions (reviewed in Avila et al., 2004; Gendron and Petrucelli, 2009) and, thus, hyperphosphorylation might free tau proteins from microtubules in the dendritic shafts, allowing tau proteins to diffuse to spines (see model in Figure 10E). Fulga et al. (2007) reported that tau-induced degeneration results in the accumulation of filamentous (F) actin, leading to direct interactions between the two proteins. F-actin is a component of dendritic spines (Fifkova and Delay, 1982; Hering and Sheng, 2001), providing another potential mechanism for hyperphosphorylated tau to mis-target to dendritic spines. Alternatively, recent studies have found that dynamic microtubules can “invade” dendritic spines to influence spine plasticity (Gu et al., 2008; Hu et al., 2008; Jaworski et al., 2009), potentially transporting bound tau into the spines.

In our *in vitro* cell culture models of tauopathy, the phosphorylation-dependent mislocalization of tau into spines was associated with suppression of basal synaptic function. This suppression was mediated, at least in part, through a postsynaptic mechanism involving loss of cell surface AMPARs but before loss of synapses (see model in Figure 10E). Beyond the impairment in basal excitatory transmission, LTP, a cellular phenomenon believed to underlie the synaptic plasticity responsible for learning and memory, was also inhibited in rTgP301L mice. These novel findings complement earlier studies using transgenic mouse models of tauopathy that express either the FTDP-17 htau mutant P301S or WT htau (Yoshiyama et al., 2007; Polydoro et al., 2009). In both models, basal synaptic transmission and LTP were impaired in the hippocampal CA1 region. Importantly, deficits in P301S mice occurred before tangle formation and neuron loss, emphasizing the importance of understanding the role synaptic dysfunction plays in tau-mediated neurodegeneration (Yoshiyama et al., 2007). Interestingly, Boekhoorn et al. (2006) reported that young transgenic mice expressing P301L htau had improved cognitive performance and increased LTP activity in the dentate gyrus, but not CA1, region of hippocampus. The authors concluded that tau hyperphosphorylation is essential for degeneration as this was absent in the young transgenic mice. Our findings complement and extend these studies by providing direct evidence that the proline-directed phosphorylation state of tau is critical for tau-mediated synaptic dysfunction. Indeed, the AP mutation reversed htau mislocalization and htau-induced decreases in excitatory synaptic transmission while the E14 mutation mimicked the deleterious effects of P301L htau. Our findings do not exclude a role for non-proline-directed S and T kinases (e.g., microtubule-affinity regulating kinases [MARKs]) in the phosphorylation-dependent mislocalization of tau. Taken together, our findings provide an important mechanistic link between phosphorylation-dependent mis-sorting of tau into postsynaptic compartments and the early synaptic impairments that precede synapse loss (see model in Figure 10E). Tau-mediated synaptic dysfunction is likely to be a key step in the transition from the asymptomatic to symptomatic phase of tauopathies, the former phase characterized by changes in functional and molecular biomarkers, the latter phase characterized by neuronal death and cognitive deficits.

Our electrophysiological and immunocytochemical experiments revealed that tau mutation or hyperphosphorylation leads to impaired trafficking or anchoring of AMPARs and NMDARs that precedes spine loss. Understanding the early pathological events preceding

synapse loss in neurodegenerative diseases is of critical relevance since synaptic loss correlates more robustly with cognitive deficits in AD than plaque or tangle load (Davies et al., 1987; Terry et al., 1991; Masliah et al., 2001; Selkoe, 2002). Most excitatory synaptic transmission is mediated through dendritic spines which are principal loci of synaptic plasticity (Hering and Sheng, 2001). Glutamatergic receptors govern the morphological plasticity of spines with NMDARs regulating the formation of new spines and AMPARs stabilizing established spines (Fischer et al., 2000). Interestingly, a recent study demonstrated that tau decreased NMDAR expression in the PSD complex, though no alterations in NMDAR-mediated currents were detected (Ittner et al., 2010). Our study complements and extends these findings to include tau-induced impairments in synaptic targeting or anchoring of AMPARs and AMPAR-mediated synaptic currents. Dendritic spine stability is compromised by loss of synaptic AMPARs, leading to spine loss (McKinney et al., 1999; Richards et al., 2005; for review, see McKinney, 2010). Despite the strong correlation between loss of spines and synaptic AMPARs, the temporal relationship between these two physiological events is not well-defined. It has also been reported that these two cellular processes can be dissociated (Sdrulla and Linden, 2007; Wang et al., 2007). Although other studies (Shahani et al., 2006; Tackenberg and Brandt, 2009) have also failed to observe tau-mediated spine loss, the state of synaptic AMPARs was not reported in these papers. Thus, we hypothesize that the absence of spine loss, despite decreased synaptic AMPARs, is due to the very early nature of the tau-induced synaptic impairments. A similar theory was proposed in a study using the APPswe/PS1dE9 transgenic mouse model of AD (Shemer et al., 2006). The relationship between Aβ-induced early synaptic dysfunction and tau-mediated global disruption of glutamate receptors remains to be determined. A recent report (Zempel et al., 2010) suggests that spines might serve as a site of convergence for amyloid beta and tau. The authors found that various cell stressors and amyloid beta oligomers induce the missorting of cytoskeletal proteins, including hyperphosphorylated tau, into the somatodendritic region which was correlated with the rapid loss of spines (≤6h). The present study further extends the Zempel et al. study by showing that phosphorylated tau proteins not only traffic to somatodendritic regions, but also aberrantly enter into dendritic spines, causing synaptic dysfunction by impeding synaptic recruitment of AMPA and NMDA receptors.

In conclusion, these findings capture what is likely the earliest synaptic dysfunction that precedes synapse loss in tauopathies and provide an important mechanistic link between proline-directed tau phosphorylation and the mislocalization of tau to dendritic spines. Our selective approach (see model in Figure 10E) to studying structurally intact mammalian neurons *in vivo* and *in vitro* revealed three results unobtainable from non-mammalian studies: 1) soluble forms of the microtubule-associated protein tau accumulate in dendritic spines, a neuronal compartment that is devoid of stable microtubules but rich in F-actin; 2) the hyperphosphorylation of tau at sites governing F-actin binding in aspiny *Drosophila* neurons directs tau to postsynaptic compartments in spiny mammalian neurons; and 3) the accumulation of tau in spines disturbs AMPAR and NMDAR trafficking or anchoring to the PSD. Our growing appreciation for the effects of other dementia-related proteins on dendritic spines (Davies et al., 1987; Selkoe, 2002; Hsieh et al., 2006; Kramer et al., 2007; Fuhrmann et al., 2007; Knobloch and Mansuy, 2008; Smith et al., 2009) highlights the importance of dendritic spines as a locus in which to study the nexus of interactions involving tau. Understanding these interactions prior to the occurrence of neuronal loss will become increasingly important as preventive strategies shift the timing of interventions to pre-degenerative phases of disease. The aberrant mislocalization of tau proteins in dendritic spines might be a novel target in these strategies.

Experimental Procedures

Materials

All chemical reagents and cell culture supplies were purchased from Sigma, Thermo-Fisher Scientific or Gibco/Invitrogen unless otherwise indicated. Antibodies used were: Tau-13 (Covance, Princeton, NJ), polyclonal PSD95 (clone c-20; Santa Cruz Biotechnology, Inc., Santa Cruz, CA), monoclonal PSD95 (Chemicon, Billerica, MA), α-tubulin (Sigma), and Tau-5 and phosphorylated S199 and T231 (Invitrogen). The polyclonal antibody against the N-terminus of GluR1 subunits of AMPARs (N-GluR1), the rabbit polyclonal antibodies against the C-terminus of GluR1 or 2/3 subunits of AMPARs and the NR1 antibody were generous gifts from Dr. Richard Huganir at the Johns Hopkins University Medical School. The Alz-50, CP-13, PG-5 and PHF-1 antibodies were generous gifts from Dr. Peter Davies at Albert Einstein College of Medicine.

Animals

Briefly, our methods for generating rTg4510 mice have been described in detail (SantaCruz et al., 2005). We generated rTg21221 mice expressing WT htau in a similar manner. To achieve regulatable expression, we utilized a system of responder and activator transgenes. Mice expressing the activator transgenes were a generous gift of Dr. Eric Kandel at Columbia University, and were successively backcrossed at least five times onto a 129S6 background strain. Responder mice were maintained in the FVB/N background strain. The WT htau cDNA encoding human 4-repeat tau lacking the amino-terminal sequences (4R0N) was modified such that the WT htau transgene (containing exons 1, 4–5, 7, 9–13, intron 13, and exon 14) driven by TRE was placed in the context of the mouse prion protein gene (*prnp*) transcribed but untranslated sequences, which were derived from the MoPrP.Xho expression vector. First, the *Sal* I fragment of a previously created WT htau transgene, including the whole htau coding sequence, was inserted into the unique *Xho* I site of MoPrP.Xho to generate prnp.WT htau. Next, the *Xba* I fragment of prnp.WT htau, including partial sequences of *prnp* introns 1 and 2, along with exons 2- 3, and the WT htau open reading frame, was cloned into the unique *Xba* I site in the inducible expression vector pTRE (Clontech, Inc., Cambridge, UK), resulting in the plasmid, pTRE.prnp.WT htau. The resultant DNA was digested with *Xho* I and *Ngo*M IV enzymes, fractionated, and purified by electroelution followed by organic extraction. Purified fragments containing a modified htau transgene were introduced by microinjection into the pronuclei of donor FVB/N embryos by standard techniques. All experiments with animals described in this study were conducted in full accordance with the American Association for the Accreditation of Laboratory Animal Care and Institutional Animal Care and Use Committee at the University of Minnesota. Every effort was made to minimize the number of animals used.

Transfection Constructs

All htau constructs were tagged with enhanced GFP (referred to as GFP) on the N-terminus and expressed in the pRK5 vector and driven by a cytomegalovirus (CMV) promoter (Clontech, Inc.). The GFP and DsRed constructs (Clontech, Inc.) were also expressed in the pRK5 vector and driven by a CMV promoter. The WT htau construct encoded human four-repeat tau lacking the N-terminal sequences (4R0N) and contained exons 1, 4 –5, 7, and 9 – 13, intron 13, and exon 14. The P301L htau construct was generated from the 4R0N WT htau sequence by mutating the proline to leucine at residue 301 with a QuikChange site-directed mutagenesis kit (Stratagene, La Jolla, CA). Using WT htau as a template, two htau constructs termed AP or E14 were generated by mutating all 14 S/P or T/P amino acid residues (T111, T153, T175, T181, S199, S202, T205, T212, T217, T231, S235, S396, S404 and S422; numbering based on the longest 441-amino acid brain isoform of htau) to alanine (AP) or glutamate (E14). The AP/P301L or E14/P301L htau construct was generated by

mutating the proline to leucine at residue 301 in AP or E14 htau, respectively. The PCR-mediated site-directed mutagenesis was confirmed by sequencing.

Neuronal rat cultures and transfections

Based on methods described in Lin et al. (2004), dissociated rat hippocampal primary neuron cultures were prepared. Briefly, a 25 mm glass coverslip (thickness, 0.08 mm) was glued over a 22 mm hole in the bottom of a 35 mm tissue-culture dish using silicone sealant. Dissociated neuronal cultures from rat hippocampi at P1–P2 were prepared. Neurons were plated onto prepared 35 mm tissue culture dishes at a density of 1×10^6 cells per dish. The age of cultured neurons was counted from the day of plating (1 DIV). Neurons at 7–10 DIV were transfected using a standard calcium phosphate precipitation method and allowed to grow to maturity (>3 weeks) to be imaged. Neurons were transfected with equivalent concentrations of plasmids encoding one of six different GFP-tagged htau constructs (WT, P301L, AP, AP/P301L, E14 or E14/P301L htau). Neurons transfected with htau constructs were co-transfected with DsRed to visualize dendritic spines. Some neurons were transfected with GFP alone to visualize dendritic spines. The culture dishes fit tightly in a homemade holding chamber on a fixed platform above an inverted epifluorescent microscope sitting on an *X*–*Y* translation stage (Burleigh Instruments, Fishers, NY).

Neuronal mouse cultures

Following the protocol described in Strasser et al. (2004), hippocampal and glial cultures were prepared from E16 and P1-2 mice, respectively. Glial cultures prepared from P1-2 mouse cortices were plated on tissue culture dishes in glial plating media (minimal essential medium [MEM] with Earle's salts, 10% fetal bovine serum [FBS] or newborn calf serum, 2 mM glutamine, 10 mM sodium pyruvate, 10 mM HEPES, 0.6% glucose, 100 U/mL penicillin and 100 μg/mL streptomyocin). For primary hippocampal neuron cultures, approximately 1.5×10^4 cells were plated on sets of 5 × 12 mm coverslips that had been previously coated with Poly-D-Lysine (100 μg/mL) + laminin (4 μg/mL) in neuronal plating media (MEM with Earle's salts, 10 mM HEPES, 10 mM sodium pyruvate, 0.5 mM glutamine, 12.5 μM glutamate, 10% FBS and 0.6% glucose). Each set of 5 coverslips was maintained in a 35 mm dish and each dish corresponded to 1 mouse. Approximately 4 hr after plating, the media was replaced with either neuronal growth medium (Neurobasal media with B27 supplement, 0.5 mM glutamine) that had been conditioned on glia for 24–48 hr immediately prior to use. Mice were genotyped by PCR analysis of tail snip lysates using transgene-specific primers.

Electrophysiology

Miniature EPSCs were recorded from cultured dissociated rat and mouse hippocampal neurons at 22–30 DIV with a glass pipette (resistance of ~5 megohm) at holding potentials of −55 mV and filtered at 1 kHz as previously described (Liao et al., 2005). Input and series resistances were checked before and after the recording of mEPSCs, which lasted 5–20 min. There were no significant difference in the series resistances and input resistance among various groups of experiments. One recording sweep lasting 200 ms was sampled for every 1 s. Neurons were bathed in artificial cerebrospinal fluid (ACSF) at room temperature (25°C) with 100 μM APV (an NMDAR antagonist), 1 μM TTX (a sodium channel blocker), and 100 μM picrotoxin (GABAa receptor antagonist), gassed with 95% O_2-5% CO_2. For experiments using rat cultures, the ACSF contained (in mM) 119 NaCl, 2.5 KCl, 5.0 $CaCl_2$, 2.5 $MgCl_2$, 26.2 $NaHCO_3$, 1 NaH_2PO_4 and 11 glucose. The frequency of mEPSCs recorded in our cultured mouse neurons is very high and, therefore, these neurons were bathed in ACSF with 0.5 mM $CaCl_2$ in order to decrease the overlap of individual mEPSC responses. The internal solution in the patch pipette contained (in mM) 100 cesium gluconate, 0.2 EGTA, 0.5 $MgCl_2$, 2 ATP, 0.3 GTP, and 40 HEPES (pH 7.2 with CsOH). All mEPSCs were

analyzed with the MiniAnalysis program designed by Synaptosoft Inc. Detection criterion for mEPSCs was set as the peak amplitude 3 pA. Each mEPSC event was visually inspected and only events with a distinctly fast-rising phase and a slow-decaying phase were accepted. The frequency and amplitude of all accepted mEPSCs were directly read out using the analysis function in the MiniAnalysis program. The averaged parameters from each neuron were treated as single samples in any further statistical analyses.

For extracellular recordings of field excitatory postsynaptic potentials (fEPSPs), hippocampal slices (350–400 μm) were prepared from 1.3 and 4.5-month old TgNeg and rTgP301L mice following standard procedures. In the recording chamber, slices were constantly perfused with ACSF solution containing (in mM) 125 NaCl, 2.5 KCl, 1.25 NaH_2PO_4, 25 $NaHCO_3$, 2 $CaCl_2$, 1 $MgCl_2$, and 10 dextrose, at near physiological temperature 30–31°C. For field recordings, a glass pipette with resistance of 1–2 megohm when filled with ACSF was placed in striatum radiatum of CA1, and a tungsten bipolar electrode was positioned to stimulate the Schaffer-collateral pathway. LTP was induced with a theta burst protocol in which 5 fEPSPs were evoked at 100 Hz to form a burst and the burst was repeated at 5 Hz.

Flow cytometry

Flow cytometry was used to measure the levels of GFP-htau protein expression in individually transfected neurons by quantifying the GFP fluorescence intensity of cells in suspension. Three week old rat neuron cultures expressing GFP-htau (WT, P301L, AP, AP/P301L, E14, E14/P301L) were washed with 1X phosphate-buffered saline (PBS) and treated with trypsin/EDTA (Sigma) for 6 min at 25°C with gentle shaking to create a single cell suspension. Cells were scraped, collected and gently triturated before addition of MEM containing 10% FBS and 2 mM glutamine to inactivate the trypsin. Cell suspensions were centrifuged for 3 min at 1000 × *g*, resuspended in 1X PBS containing 2% FBS, filtered with a 5 mL polystyrene round bottom tube with a cell strainer cap (Becton Dickinson, San Jose, CA) and stored at 4°C until flow cytometry analysis. Flow cytometry/sorting was done on a FACSVantage DIVA SE (Becton Dickinson) flow cytometer using Diva software (version 5.0.2). The fluorescent DNA marker 7-aminoactinomycin D (7-AAD; 1:500; Invitrogen) was used to isolate live cells. The flow cytometry data were analyzed and scatter profiles for fluorescence intensities plotted using Flowjo software (Treestar, Ashland, OR, version 8.8.6).

Tau Immunoprecipitation

Three week old rat neuron cultures expressing GFP-htau (WT, P301L, AP, AP/P301L, E14, E14/P301L) were lysed (50 mM Tris-HCl, 150 mM NaCl, 1 mM EDTA, 1.5% Triton X-100, 0.1% Na deoxycholate, phosphatase inhibitors [phenylmethylsulfonyl fluoride, phenenthroline monohydrate and phosphatase inhibitor cocktails I and II; 1:1000, Sigma] and protease inhibitor cocktail [1:100; Sigma]; 30 min at 4°C on shaker), scraped and lysates were collected for determination of total protein concentration by the BCA protein assay. An aliquot of each sample (450 μg) was diluted in 1 mL of dilution buffer (50 mM Tris-HCl, 150 mM NaCl, pH 7.4 and freshly added protease and phosphatase inhibitors) and immunodepleted with 150 μL Protein A and 150 μL Protein G for 1 hr at 4°C. Immunodepleted samples were incubated with 30 μg Tau-13 antibody and 100 μL protein G sepharose beads overnight at 4°C. The next day, beads were washed with buffer A (50 mM Tris-HCl, 0.1% Triton X-100, 300 mM NaCl, 1 mM EDTA) for 20 min at 4°C followed by a wash with buffer B (50 mM Tris-HCl, 0.1% Triton X-100, 150 mM NaCl, 1 mM EDTA) for 20 min at 4°C. Sample was eluted off the beads using 1X sodium dodecyl sulfate (SDS) loading buffer, heated to 95°C for 10 min and analyzed by western blot analysis as described using the Tau-13 (total tau), pS199, pT231 and Alz-50 antibodies.

Brain fractionation and western blot analyses

Preparation of postsynaptic densities from mouse brains was performed based on the procedures of Cheng et al. (2006). Briefly, PSD fractions were prepared from mouse forebrains at 4°C. Forebrains were collected from adult mice and homogenized in ice-cold Buffer A (6 mM Tris [pH 8.0], 0.32 M sucrose, 1 mM $MgCl_2$, 0.5 mM $CaCl_2$, phosphatase inhibitors [phenylmethylsulfonyl fluoride, phenenthroline monohydrate and phosphatase inhibitor cocktails I and II; 1:100, Sigma] and protease inhibitor cocktail [1:100; Sigma]). The resulting extract was centrifuged at low speed (1,400 × *g* for 10 min) to collect the first supernatant (S1). The pellet (P1) was re-extracted and homogenized with Buffer A and centrifuged at 710 × *g* for 10 min. This supernatant (S1') was pooled with the S1 supernatant and then centrifuged at 710 × *g* for 10 min. Then, the supernatant was removed and centrifuged at 13,800 × *g* for 12 min to isolate the S2 supernatant used for western blotting. The S2 fraction contains both pre- and postsynaptic proteins. The pellet (P2) was resuspended and homogenized in Buffer B (0.32 M sucrose and 6 mM Tris [pH 8.0] with the same phosphatase and protease inhibitors). This homogenate was loaded onto a discontinuous sucrose gradient (0.85/1/1.15 M in 6 mM Tris [pH 8.0]), and centrifuged at 82,500 × *g* for 2 h. The synaptosome fraction (Syn) between 1 M and 1.15 M sucrose was collected and adjusted to 2 mL with Buffer B. An equal volume of Buffer C (12 mM Tris [pH 8.0] and 1% Triton X-100) was added, mixed for 15 min, and centrifuged at 32,800 × *g* for 20 min. The PSD protein pellet (PSD-1) was resuspended in 40 mM Tris (pH 8.0). The protein concentration was determined by Pierce BCA protein assay using bovine serum albumin as standard. For Western blot detection of proteins of interest in the S2 and PSD-1 fractions of mouse forebrains, protein-corrected (BCA assay) samples were diluted in reducing sample buffer, electrophoresed on 10% Tris-HCl gels (Bio-Rad, Hercules, CA), and transferred onto 0.45 μm polyvinylidene difluoride membranes (Millipore, Billerica, MA). Briefly, blots were processed with the primary antibody (Tau-13, α-tubulin or polyclonal PSD95) and visualized using enhanced chemiluminescence reagents (Pierce, Rockford, IL), followed by exposure onto Kodak hyperfilm. Band density from film exposed within the linear range was measured using OptiQuant 3.0 software (Packard Instrument Co., Downers Grove, IL).

Immunohistochemistry

Immunohistochemical detection of total and phosphorylated tau species in transgenic and control mice was performed as previously described (Ramsden et al., 2005). Briefly, hemibrains were immersion fixed in 10% formalin for 24–48 h and embedded in paraffin. Serial sections were cut at 5 μm using a microtome, mounted onto CapGap slides (Thermo-Fisher), and rehydrated according to standard protocols. Mounted slides were pretreated with a citrate buffer (pH 6.0) in a Black & Decker (Owings, MD) steamer for 30 min, with a 10 min cool down. Standard 2 d immunostaining procedures using peroxidase-labeled streptavidin and DAB chromagen on an automated TechMate 500 capillary gap immunostainer (Ventana Medical Systems, Tucson, AZ) were used with antibodies directed against total human and mouse tau (Tau-5) or human tau hyperphosphorylated at S202, S396/S404, and S409 (CP-13, PHF-1, PG-5 respectively). Photomicrographs of hippocampal and cortical neurons were captured at three different magnifications (x5, x10 and x40) with a Zeiss Axioskop microscope coupled to a CCD camera and processed and assembled in Adobe Photoshop.

Immunolabeling glutamate receptors and PSD95

As previously described (Liao et al., 1999), a green fluorescent dye-conjugated rabbit polyclonal antibody against the N-terminus of GluR1 subunits of AMPARs was added to culture media of living mouse neurons at a concentration of 1:100 to label surface AMPARs. Neurons were incubated with the antibody-containing media for 1 hour at 37°C and were

subsequently fixed and permeabilized successively with 4% paraformaldehyde/4% sucrose in 1X PBS (25°C, 20 min), −20°C 100% methanol (4°C, 10 min) and 0.2% Triton X-100 (25°C, 10–20 min). The neurons were then incubated with a mouse anti-PSD95 monoclonal antibody (1:100) in 10% donkey serum at 4°C overnight. The PSD95 protein is a widely-used marker of dendritic spines, because it is highly enriched in postsynaptic densities. Immunocytochemical detection of total GluR1 and 2/3 AMPAR subunits with two separate C-terminus antibodies and NR1 with a N-terminus antibody was performed in a similar manner except that all primary antibodies were added after the fixation and permeabilization of the neurons and, therefore, both surface and intracellular receptors were labeled (Figure 6). Primary antibodies were visualized with the appropriate secondary antibodies conjugated to either FITC or rhodamine (Jackson Immunoresearch Laboratories, West Grove, PA).

Image analysis of fixed and living neurons

Coverslips of fixed mouse neurons or rat neurons co-transfected with various GFP-tagged tau constructs and DsRed (or GFP alone) were photographed on an inverted Nikon epifluorescent microscope with a 60X oil lens and a computerized focus motor at 21–35 DIV. All digital images were photographed and processed with MetaMorph Imaging System (Universal Imaging Corporation, West Chester, PA). All images of fixed and live neurons were taken as stacks (15 planes at 0.5 micron increments) and processed by deconvolution analyses using the MetaMorph software with the nearest planes and averaged into one single image. A dendritic protrusion with an expanded head that was 50% wider than its neck was defined as a spine. The number of spines from one neuron was counted manually and normalized per 100 μm dendritic length. To measure the dendritic fluorescence intensity of individual rat hippocampal neurons, living neurons were photographed and processed with MetaMorph software as described above. Then, using Image J software (Image J 1.42q Software, National Institutes of Health, http://rsb.info.nih.gov/ij), the fluorescent pixel intensity along a user-defined line drawn at three different random positions across a GFP htau-transfected dendrite was measured as distance along the x-axis plotted against pixel gray value on the y-axis and expressed as area under a curve. The area under the curve above baseline was measured and represented as fluorescent pixel intensity using Image J software. To estimate the amount of glutamate receptors in dendritic spines, fixed mouse neurons immunoreactive for PSD95 and a GluR antibody (N-GluR1, GluR1 detected with a C-terminus antibody, GluR2/3, NR1) were photographed and processed with MetaMorph software as described above. Then, immunoreactive clusters of PSD95 were auto-selected using the MetaMorph software and the location of these clusters was transferred to images displaying glutamate receptor immunoreactivity on the same neuron. PSD95 immunoreactivity was used to identify dendritic spines. A cursor was placed in the center of the glutamate receptor clusters in dendritic spines to estimate glutamate receptor immunoreactivity as fluorescent pixel intensity in the spines (value Y1). Another cursor was placed in an adjacent dendritic shaft to measure glutamate receptor fluorescent pixel intensity (value Y2) and the ratio of glutamate receptor immunoreactive fluorescence intensity in spines/dendrites (Y1/Y2) was plotted on the Y-axis.

Behavioral Testing

Spatial reference memory was measured using the Morris water-maze with a protocol tailored for the rapid learning of the 129FVBF1 mice (Westerman et al., 2002; Ramsden et al., 2005). Mice were prehandled for 10 days during the 2 weeks preceding Morris water-maze testing. Prehandling consisted of a 20 s exposure to water at a depth of 1 cm and was designed to acclimatize the mice to the introduction and removal from the testing pool. At each age tested, mice received visible platform training for three days, six trials per day, followed by hidden platform training for six days, four trials per day. Four probe trials of 30 s duration were performed 20 h after eight, 12, 16, and 24 hidden training trials. The mean

platform crossing index of all four probes was calculated. All trials were monitored using a computerized tracking system (Noldus EthoVision 3.0; Noldus Information Technology, Wageningen, The Netherlands), and performance measures were extracted using Wintrack (Wolfer et al., 2001).

Statistical Analyses

Statistical analysis utilized Student's t-tests, analysis of variance (ANOVA) and repeated-measures ANOVA. Post-hoc comparisons were performed using Fisher's PLSD or Bonferroni correction to compare the difference between the means of experimental groups. The Kolmogorov-Smirnov test was used to examine the difference between cumulative frequency distributions in the electrophysiological experiments. Repeated-measures ANOVA was used to examine differences in spatial reference memory performance and transgenic status served as the between-subject variable, while training block served as the within-subject variable. Statistical significance is $p < 0.05$. All data are expressed as mean ± SEM.

Supplementary Material

Refer to Web version on PubMed Central for supplementary material.

Acknowledgments

We thank P. Higgins, S. Liu, J. Paulson, M. Schmidt, L. Kemper, T. Moroni, N. Anderson and B. Dummer for expert technical assistance, Dr. R. Huganir (Johns Hopkins University) for the glutamate receptor antibodies, Dr. P. Davies (Albert Einstein College of Medicine) for the tau antibodies and Dr. E. Kandel (Columbia University) for the activator mice. We would like to acknowledge the assistance of N. Shah and the Flow Cytometry Core Facility of the Masonic Cancer Center at the University of Minnesota, a comprehensive cancer center designated by the National Cancer Institute, supported in part by P30 CA77598. Sources of funding for this study include B. Grossman and her family, the American Health Assistance Foundation (D.L.) and the NIH (R01-DA020582, K02-DA025048 to D.L.; R01-NS049178 to L.M.L.; T32-DA007234 to R.D.P.; R01-NS049129 to L.L.Y.; T32 DA022616-02 to M.N.R.; R01-AG026252, R01-NS063214 to K.H.A.).

REFERENCES

Arvanitakis Z, Witte RJ, Dickson DW, Tsuboi Y, Uitti RJ, Slowinski J, Hutton ML, Lin S-C, Boeve BF, Cheshire WP, Pooley RA, Liss JM, Caviness JN, Strongosky AJ, Wszolek ZK. Clinical-pathologic study of biomarkers in FTDP-17 (PPND family with N279K *tau* mutation). Parkinsonism Relat. Disord. 2007; 13:230–239. [PubMed: 17196872]

Avila J, Lucas JJ, Perez M, Hernandez F. Role of tau protein in both physiological and pathological conditions. Physiol. Rev. 2004; 84:361–384. [PubMed: 15044677]

Bertrand J, Plouffe V, Senechal P, Leclerc N. The pattern of human tau phosphorylation is the result of priming and feedback events in primary hippocampal neurons. Neuroscience. 2010; 168:323–334. [PubMed: 20394726]

Boekhoorn K, Terwel D, Biemans B, Borghgraef P, Wiegert O, Ramakers GJA, de Vos K, Krugers H, Tomiyama T, Mori H, Joels M, van Leuven F, Lucassen PJ. Improved long-term potentiation and memory in young tau-P301L transgenic mice before onset of hyperphosphorylation and tauopathy. J. Neurosci. 2006; 26:3514–3523. [PubMed: 16571759]

Brandt R, Hundelt M, Shahani N. Tau alteration and neuronal degeneration in tauopathies: mechanisms and models. Biochim. Biophys. Acta. 2005; 1739:331–354. [PubMed: 15615650]

Buee L, Bussiere T, Buee-Scherrer V, Delacourte A, Hof PR. Tau protein isoforms, phosphorylation and role in neurodegenerative disorders. Brain Res. Rev. 2000; 33:95–130. [PubMed: 10967355]

Cheng D, Hoogenraad CC, Rush J, Ramm E, Schlager MA, Duong DM, Xu P, Wijayawardana SR, Hanfelt J, Nakagawa T, Sheng M, Peng J. Relative and absolute quantification of postsynaptic density proteome isolated from rat forebrain and cerebellum. Mol. Cell. Proteomics. 2006; 5:1158–1170. [PubMed: 16507876]

Davies CA, Mann DM, Sumpter PQ, Yates PO. A quantitative morphometric analysis of the neuronal and synaptic content of the frontal and temporal cortex in patients with Alzheimer's disease. J. Neurol. Sci. 1987; 78:151–164. [PubMed: 3572454]

Dixit R, Ross JL, Goldman YE, Holzbaur ELF. Differential regulation of dynein and kinesin motor proteins by tau. Science. 2008; 319:1086–1089. [PubMed: 18202255]

Eckermann K, Mocanu M-M, Khlistunova I, Biernat J, Nissen A, Hofmann A, Schonig K, Bujard H, Haemisch A, Mandelkow E, Zhou L, Rune G, Mandelkow E-M. The β-propensity of tau determines aggregation and synaptic loss in inducible mouse models of tauopathy. J. Biol. Chem. 2007; 282:31755–31765. [PubMed: 17716969]

Fifkova E, Delay RJ. Cytoplasmic actin in neuronal processes as a possible mediator of synaptic plasticity. J. Cell Biol. 1982; 95:345–350. [PubMed: 6890558]

Fischer M, Kaech S, Wagner U, Brinkhaus H, Matus A. Glutamate receptors regulate actin-based plasticity in dendritic spines. Nat. Neurosci. 2000; 3:887–894. [PubMed: 10966619]

Fuhrmann M, Mitteregger G, Kretzschmar H, Herms J. Dendritic pathology in prion disease starts at the synaptic spine. J. Neurosci. 2007; 27:6224–6233. [PubMed: 17553995]

Fulga TA, Elson-Schwab I, Khurana V, Steinhilb ML, Spires TL, Hyman BT, Feany MB. Abnormal bundling and accumulation of F-actin mediates tau-induced neuronal degeneration *in vivo*. Nat. Cell Biol. 2007; 9:139–148. [PubMed: 17187063]

Gendron TF, Petrucelli L. The role of tau in neurodegeneration. Mol. Neurodegener. 2009; 4:13–31. [PubMed: 19284597]

Gong C-X, Liu F, Grundke-Iqbal I, Iqbal K. Post-translational modifications of tau protein in Alzheimer's disease. J. Neural Transm. 2005; 112:813–838. [PubMed: 15517432]

Gu J, Firestein BL, Zheng JQ. Microtubules in dendritic spine development. J. Neurosci. 2008; 28:12120–12124. [PubMed: 19005076]

He HJ, Wang XS, Pan R, Want DL, Liu MN, He RQ. The proline-rich domain of tau plays a role in interactions with actin. BMC Cell Biol. 2009; 10:81–92. [PubMed: 19895707]

Hering H, Sheng M. Dendritic spines: structure, dynamics and regulation. Nat. Rev. Neurosci. 2001; 2:880–888. [PubMed: 11733795]

Hsieh H, Boehm J, Sato C, Iwatsubo T, Tomita T, Sisodia S, Malinow R. AMPAR removal underlies Aβ-induced synaptic depression and dendritic spine loss. Neuron. 2006; 52:831–843. [PubMed: 17145504]

Hu X, Viesselmann C, Nam S, Merriam E, Dent EW. Activity-dependent dynamic microtubule invasion of dendritic spines. J. Neurosci. 2008; 28:13094–13105. [PubMed: 19052200]

Isaac JTR, Nicoll RA, Malenka RC. Evidence for silent synapses: implications for the expression of LTP. Neuron. 1995; 15:427–434. [PubMed: 7646894]

Ittner LM, Ke YD, Delerue F, Bi M, Gladbach A, Eersel Jv, Wolfing H, Chieng BC, Christie MJ, Napier IA, Eckert A, Staufenbiel M, Hardeman E, Gotz J. Dendritic function of tau mediates amyloid-β toxicity in Alzheimer's disease mouse models. Cell. 2010; 142:387–397. [PubMed: 20655099]

Jaworski J, Kapitein LC, Gouveia SM, Dortland BR, Wulf PS, Grigoriev I, Camera P, Spangler SA, Di Stefano P, Demmers J, Krugers H, Defilippi P, Akhmanova A, Hoogenraad CC. Dynamic microtubules regulate dendritic spine morphology and synaptic plasticity. Neuron. 2009; 61:85–100. [PubMed: 19146815]

Knobloch M, Mansuy IM. Dendritic spine loss and synaptic alterations in Alzheimer's disease. Mol. Neurobiol. 2008; 37:73–82. [PubMed: 18438727]

Kramer ML, Schulz-Schaeffer WJ. Presynaptic α-synuclein aggregates, not Lewy bodies, cause neurodegeneration in dementia with Lewy bodies. J. Neurosci. 2007; 27:1405–1410. [PubMed: 17287515]

Liao D, Hessler NA, Malinow R. Activation of postsynaptically silent synapses during pairing-induced LTP in CA1 region of hippocampus slice. Nature. 1995; 375:400–404. [PubMed: 7760933]

Liao D, Zhang X, O'Brien R, Ehlers MD, Huganir RL. Regulation of morphological postsynaptic silent synapses in developing hippocampal neurons. Nat. Neurosci. 1999; 2:37–43. [PubMed: 10195178]

Liao D, Lin H, Law PY, Loh HH. Mu-opioid receptors modulate the stability of dendritic spines. Proc. Natl. Acad. Sci. U.S.A. 2005; 102:1725–1730. [PubMed: 15659552]

Lin H, Huganir R, Liao D. Temporal dynamics of NMDA receptor-induced changes in spine morphology and AMPA receptor recruitment to spines. Biochem. Biophys. Res. Commun. 2004; 316:501–511. [PubMed: 15020245]

Luna-Munoz J, Chavez-Macias L, Garcia-Sierra F, Mena R. Earliest stages of tau conformational changes are related to the appearance of a sequence of specific phospho-dependent tau epitopes in Alzheimer's disease. J. Alzheimers Dis. 2007; 12:365–375. [PubMed: 18198423]

Malinow R, Malenka RC. AMPA receptor trafficking and synaptic plasticity. Annu. Rev. Neurosci. 2002; 25:103–126. [PubMed: 12052905]

Mandelkow E-M, Stamer K, Vogel R, Thies E, Mandelkow E. Clogging of axons by tau, inhibition of axonal traffic and starvation of synapses. Neurobiol. Aging. 2003; 24:1079–1085. [PubMed: 14643379]

Masliah E, Mallory M, Alford M, DeTeresa R, Hansen LA, McKeel DW Jr, Morris JC. Altered expression of synaptic proteins occurs early during progression of Alzheimer's disease. Neurology. 2001; 56:127–129. [PubMed: 11148253]

Maurage C-A, Sergeant N, Ruchoux M-M, Hauw J-J, Delacourte A. Phosphorylated serine 199 of microtubule-associated protein tau is a neuronal epitope abundantly expressed in youth and an early marker of tau pathology. Acta Neuropathol. 2003; 105:89–97. [PubMed: 12536218]

McKinney RA, Capogna M, Durr R, Gahwiler BH, Thompson SM. Miniature synaptic events maintain dendritic spines via AMPA receptor activation. Nat. Neurosci. 1999; 2:44–49. [PubMed: 10195179]

McKinney RA. Excitatory amino acid involvement in dendritic spine formation, maintenance and remodeling. J. Physiol. (London). 2010; 588:107–116. [PubMed: 19933758]

Newpher TM, Ehlers MD. Glutamate receptor dynamics in dendritic microdomains. Neuron. 2008; 58:472–497. [PubMed: 18498731]

Oddo S, Vasilevko V, Caccamo A, Kitazawa M, Cribbs DH, LaFerla FM. Reduction of soluble Aβ and tau, but not soluble Aβ alone, ameliorates cognitive decline in transgenic mice with plaques and tangles. J. Biol. Chem. 2006; 281:39413–39423. [PubMed: 17056594]

Papasozomenos, SCh; Binder, LI. Phosphorylation determines two distinct species of tau in the central nervous system. Cell Motil. Cytoskeleton. 1987; 8:210–226. [PubMed: 2446784]

Petrie EC, Cross DJ, Galasko D, Schellenberg GD, Raskind MA, Peskind ER, Minoshima S. Preclinical evidence of Alzheimer changes: Convergent cerebrospinal fluid biomarker and fluorodeoxyglucose positron emission tomography findings. Arch. Neurol. 2009; 66:632–637. [PubMed: 19433663]

Polydoro M, Acker CM, Duff K, Castillo PE, Davies P. Age-dependent impairment of cognitive and synaptic function in the htau mouse model of tau pathology. J. Neurosci. 2009; 29:10741–10749. [PubMed: 19710325]

Ramsden M, Kotilinek L, Forster C, Paulson J, McGowan E, SantaCruz K, Guimaraes A, Yue M, Lewis J, Carlson G, Hutton M, Ashe KH. Age-dependent neurofibrillary tangle formation, neuron loss, and memory impairment in a mouse model of human tauopathy (P301L). J. Neurosci. 2005; 25:10637–10647. [PubMed: 16291936]

Richards DA, Mateos JM, Hugel S, de Paola V, Caroni P, Gahwiler BH, McKinney RA. Glutamate induces the rapid formation of spine head protrusions in hippocampal slice cultures. Proc. Natl. Acad. Sci. USA. 2005; 102:6166–6171. [PubMed: 15831587]

Rocher AB, Crimins JL, Amatrudo JM, Kinson MS, Todd-Brown MA, Lewis J, Luebke JI. Structural and functional changes in tau mutant mice neurons are not linked to the presence of NFTs. Exp. Neurol. 2010; 223:385–393. [PubMed: 19665462]

SantaCruz K, Lewis J, Spires T, Paulson J, Kotilinek L, Ingelsson M, Guimaraes A, DeTure M, Ramsden M, McGowan E, Forster C, Yue M, Orne J, Janus C, Mariash A, Kuskowski M, Hyman B, Hutton M, Ashe KH. Tau suppression in a neurodegenerative mouse model improves memory function. Science. 2005; 309:476–481. [PubMed: 16020737]

Sdrulla AD, Linden DJ. Double dissociation between long-term depression and dendritic spine morphology in cerebellar Purkinje cells. Nat. Neurosci. 2007; 10:546–548. [PubMed: 17435753]

Selkoe D. Alzheimer's disease is a synaptic failure. Science. 2002; 298:789–791. [PubMed: 12399581]

Shahani N, Subramaniam S, Wolf T, Tackenberg C, Brandt R. Tau aggregation and progressive neuronal degeneration in the absence of changes in spine density and morphology after targeted expression of Alzheimer's disease-relevant tau constructs in organotypic hippocampal slices. J. Neurosci. 2006; 26:6103–6114. [PubMed: 16738255]

Shemer I, Holmgren C, Min R, Fulop L, Zilberter M, Sousa KM, Farkas T, Hartig W, Penke B, Burnashev N, Tanila H, Zilberter Y, Harkany T. Non-fibrillar β-amyloid abates spike-timing-dependent synaptic potentiation at excitatory synapses in layer 2/3 of the neocortex by targeting postsynaptic AMPA receptors. Eur. J. Neurosci. 2006; 23:2035–2047. [PubMed: 16630051]

Smith DL, Pozueta J, Gong B, Arancio O, Shelanski M. Reversal of long-term dendritic spine alterations in Alzheimer disease models. Proc. Natl. Acad. Sci. U.S.A. 2009; 106:16877–16882. [PubMed: 19805389]

Steinhilb ML, Dias-Santagata D, Mulkearns EE, Shulman JM, Biernat J, Mandelkow E-M, Feany MB. S/P and T/P phosphorylation is critical for tau neurotoxicity in *Drosophila*. J. Neurosci. Res. 2007a; 85:1271–1278. [PubMed: 17335084]

Steinhilb ML, Dias-Santagata D, Fulga TA, Felch DL, Feany MB. Tau phosphorylation sites work in concert to promote neurotoxicity in vivo. Mol. Biol. Cell. 2007b; 18:5060–5068. [PubMed: 17928404]

Strasser GA, Rahim NA, VanderWaal KE, Gertler FB, Lanier LM. Arp2/3 is a negative regulator of growth cone translocation. Neuron. 2004; 43:81–94. [PubMed: 15233919]

Tackenberg C, Brandt R. Divergent pathways mediate spine alterations and cell death induced by amyloid-β, wild-type tau, and R406W tau. J. Neurosci. 2009; 29:14439–14450. [PubMed: 19923278]

Terry RD, Masliah E, Salmon DP, Butters N, DeTeresa R, Hill R, Hansen LA, Katzman R. Physical basis of cognitive alterations in Alzheimer's disease: synapse loss is the major correlate of cognitive impairment. Ann. Neurol. 1991; 30:572–580. [PubMed: 1789684]

Wang, X-b; Yang, Y.; Zhou, Q. Independent expression of synaptic and morphological plasticity associated with long-term depression. J. Neurosci. 2007; 27:12419–12429. [PubMed: 17989307]

Westerman MA, Cooper-Blacketer D, Mariash A, Kotilinek L, Kawarabayashi T, Younkin LH, Carlson GA, Younkin SG, Ashe KH. The relationship between Aβ and memory in the Tg2576 mouse model of Alzheimer's disease. J. Neurosci. 2002; 22:1858–1867. [PubMed: 11880515]

Wolfer DP, Madani R, Valenti P, Lipp HP. Extended analysis of path data from mutant mice using the public domain software Wintrack. Physiol. Behav. 2001; 73:745–753. [PubMed: 11566208]

Yoshiyama Y, Higuchi M, Zhang B, Huang S-M, Iwata N, Saido TC, Maeda J, Suhara T, Trojanowski JQ, Lee VM-Y. Synapse loss and microglial activation precede tangles in a P301S tauopathy mouse model. Neuron. 2007; 53:337–351. [PubMed: 17270732]

Zempel H, Thies E, Mandelkow E, Mandelkow E-M. Aβ oligomers cause localized Ca^{2+} elevation, missorting of endogenous tau into dendrites, tau phosphorylation, and destruction of microtubules and spines. J. Neurosci. 2010; 30:11938–11950. [PubMed: 20826658]

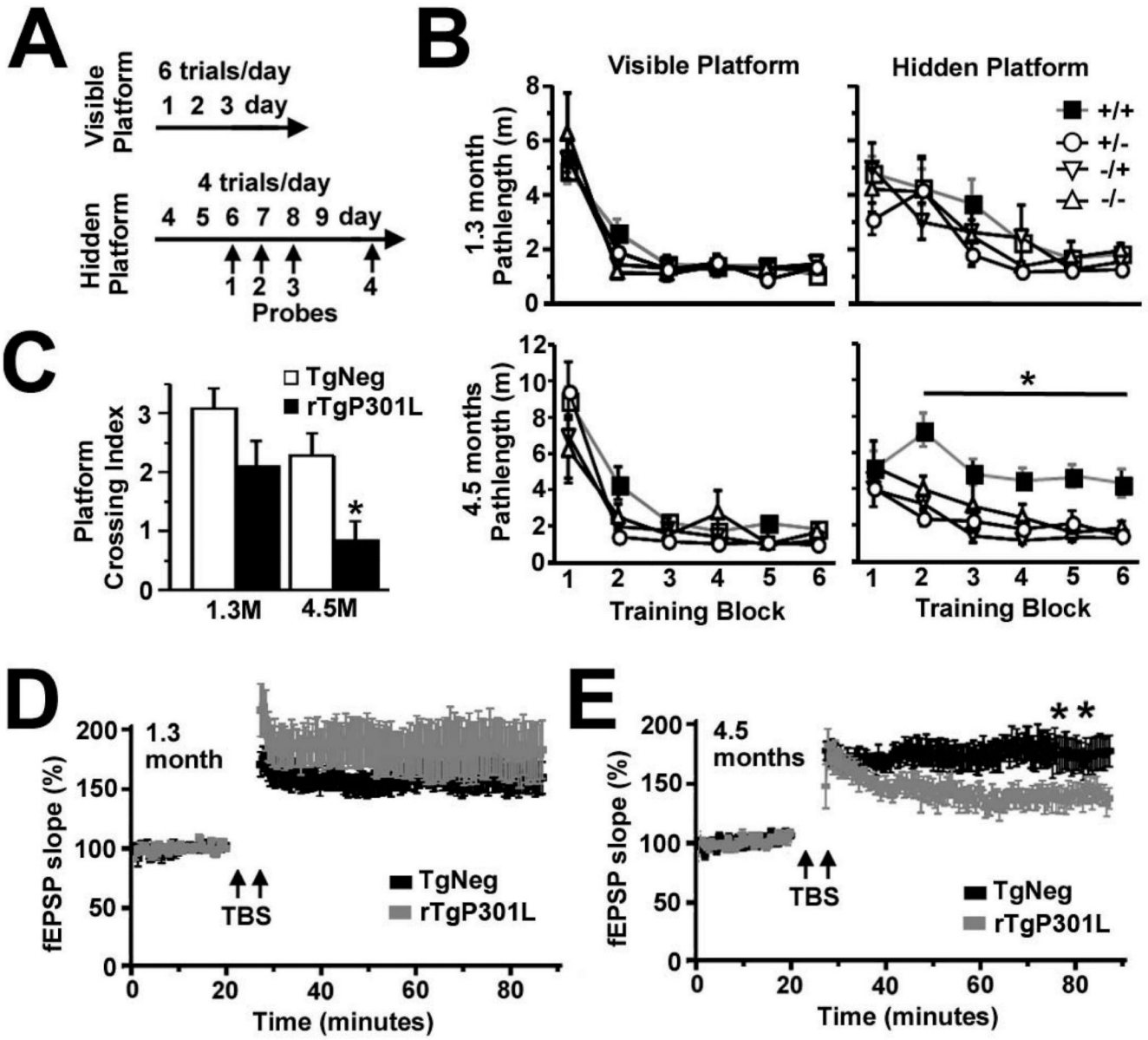

Figure 1. Memory and synaptic plasticity in rTgP301L mice

(A) Timeline of sequential training and testing in the Morris water maze as previously described (Westerman et al., 2002; Ramsden et al., 2005). (B) No deficits were observed in locating the visible platform at any age. Only 4.5-month old rTgP301L mice showed a significant deficit in learning to locate the hidden platform. (C) rTgP301L mice at 4.5 but not 1.3 months (M) showed impaired retention of spatial reference memory as assayed by the platform crossing index. n = 12 rTg mice at each age and n = 4 mice for each TgNeg group at each age (B) for a total of 12 mice for pooled TgNeg group (C). (D) There was no difference in theta burst stimuli (TBS)-induced long term potentiation (LTP) of field excitatory postsynaptic potentials (fEPSPs) in the CA1 hippocampal subfield between rTgP301L and TgNeg littermates at 1.3 months. (E) LTP was impaired in 4.5-month old rTgP301L mice. n = 10 brain slices from each group in 4.5-month old mice (n = 6 animals/genotype); n = 14 rTg brain slices and n = 12 control slices from 1.3-month old mice (n = 6 animals/genotype). +/+, rTgP301L mice; +/−, −/+, or −/−, TgNeg control mice that express

the activator, responder, or neither transgene, respectively. For experiments in panels C–E, the TgNegcontrolmicewerecombinedintoonegroupdesignatedasTgNegsincetherewasno difference between TgNeg subpopulations in cognitive performance (B). M, months; m, meters. Repeated-measures ANOVA, *$p < 0.05$, **$p < 0.01$.

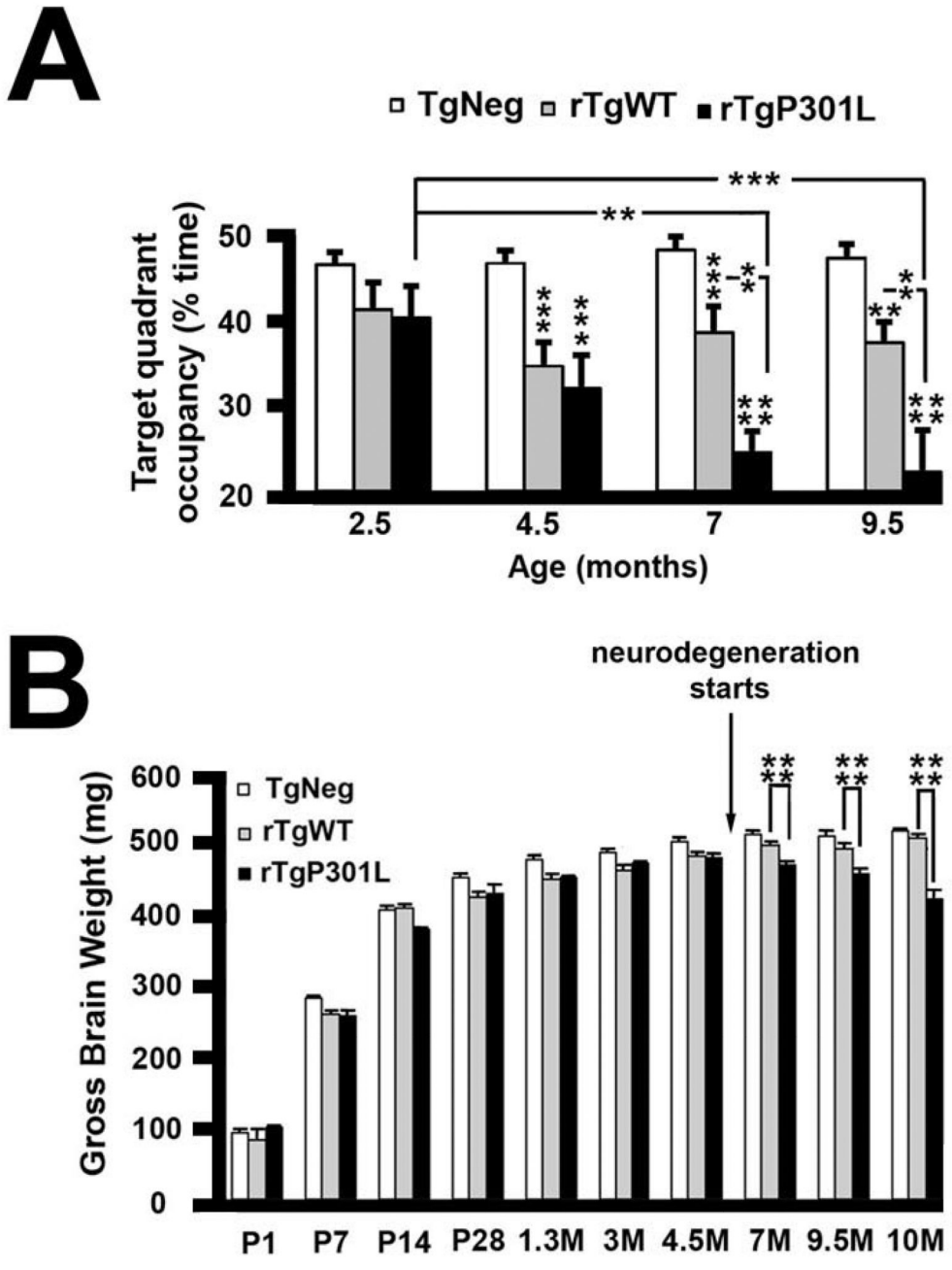

Figure 2. Lack of age-dependent memory deficits and neurodegeneration in rTgWT mice

(A) rTgWT mice were longitudinally tested in the Morris water maze and compared to previously published data from the rTgP301L mice (Ramsden et al., 2005) [2.5M–9.5M n = 52 TgNeg, n = 17 rTgWT and n = 9 rTgP301L]. rTgWT mice showed deficits in performance in the Morris water maze compared to TgNeg mice. Deficits in rTgWT mice remained stable for several months, while deficits in rTgP301L mice became more severe with increasing age. Although rTgWT spent less time swimming in the target quadrant during probe trials compared to TgNeg mice, only the rTgP301L mice exhibited an age-related decline. Repeated measures ANOVA data are as follows: transgene: $F(2,225) = 34.09$, $p < 0.0001$; age versus transgene: $F(6,225) = 3.61$, $p < 0.01$; age, TgNeg mice:

F(3,153) = 0.345, p = 0.79; age, rTgWT mice: F(3,48) = 1.518, p = 0.22; age, rTgP301L mice: F(3,24) = 5.82. (B) While both rTgWT and rTgP301L mice exhibited a significant decrease in whole brain weight early in life (1.3–4.5 months of age), suggestive of a developmental delay, the rTgP301L mice also exhibited neurodegeneration as evidenced by a progressive decrease in whole brain weight later in life (7–10 months of age). Due to small sample numbers at some ages, mice were binned into P1-P28, 1.3M-4.5M, and 7M-10M. Although there was a trend towards decreased brain weights at P1-P28, this was not statistically different. Data for transgene ANOVA are as follows: P1-P28: F(2,82) = 0.524, p = 0.5939; 1.3M-4.5M: F(2,156) = 14.564, p < 0.0001; 7M-10M: F(2,141) = 66.957, p < 0.0001. Sample sizes for TgNeg, rTgWT, rTgP301L, respectively, are as follows: P1, n = 13, n = 2, n = 2; P7, n = 20, n = 3, n = 2; P14, n = 17, n = 4, n = 4; P28, n = 9, n = 5, n = 4; 1.3M, n = 18, n = 5, n = 12; 3M, n = 35, n = 15, n = 14; 4.5M, n = 26, n = 21, n = 13; 7M, n = 19, n = 14, n = 19; 9.5M, n = 12, n = 9, n = 12; 10M, n = 36, n = 9, n = 14. M, months; **p < 0.01, ***p < 0.001, ****p < 0.0001. See also Figure S1 for details on the creation and characterization of rTgWT mice.

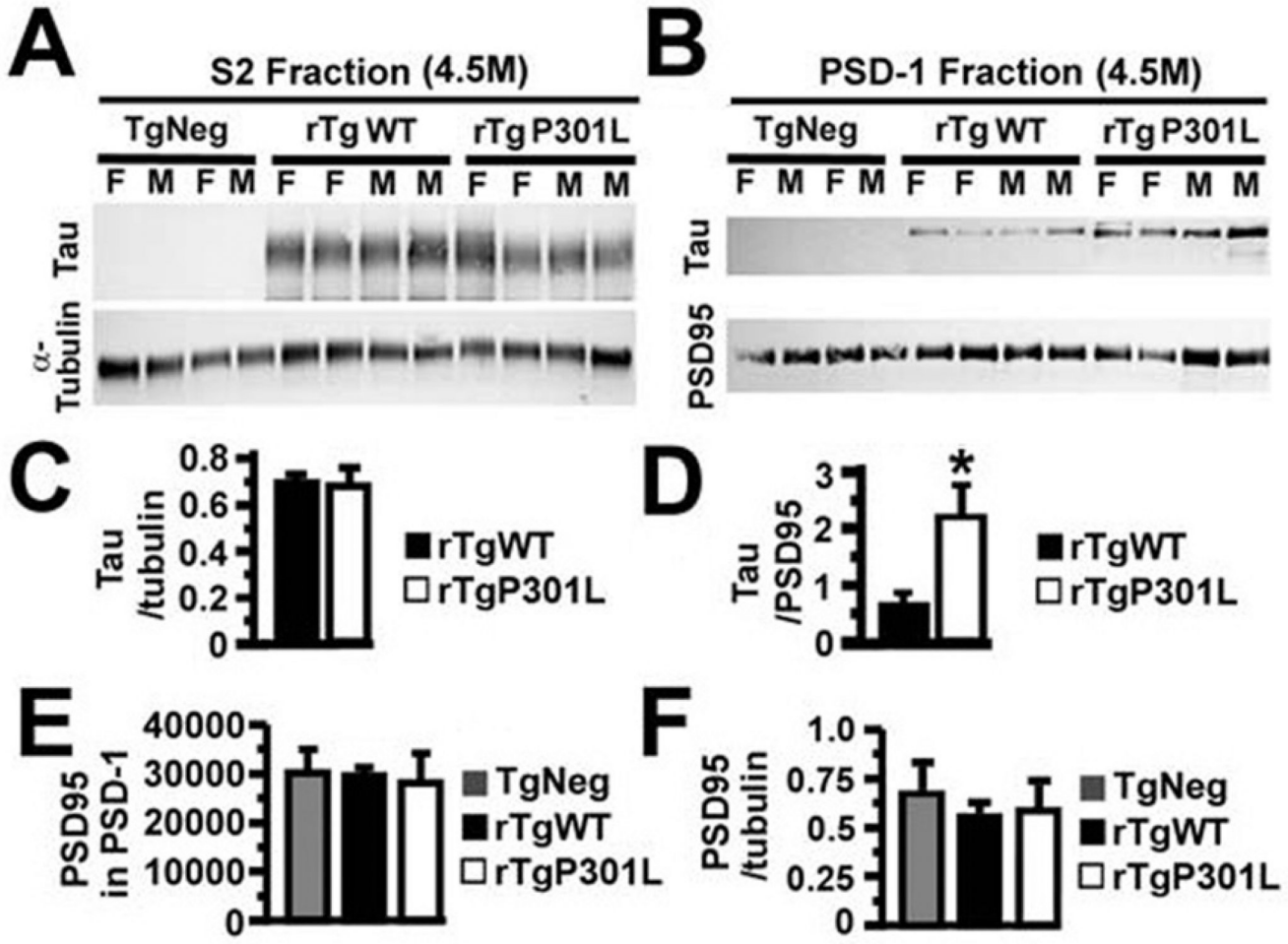

Figure 3. Human tau levels in the forebrains of rTgP301L and rTgWT mice

(A) Tubulin and htau proteins in the S2 fraction of forebrains from 4.5-month old (4.5M) TgNeg, rTgWT and rTgP301L mice. (B) PSD95 and htau proteins in the PSD-1 fractions of forebrains from the animals in (A). (C) There was no difference in the normalized levels of htau expression between rTgWT and rTgP301L mice in the S2 fraction. (D) There was more htau, normalized to PSD95, in the PSD-1 fractions of rTgP301L mice. (E) There was no difference in the levels of PSD95 between TgNeg, rTgWT and rTgP301L mice. (F) Levels of PSD95 did not change in relation to a-tubulin between TgNeg, rTgWT and rTgP301L mice. n = 9–10 mice per group. M, male; F, female. t-test (C, D), ANOVA followed by Bonferroni post-hoc analysis (E), *$p < 0.05$.

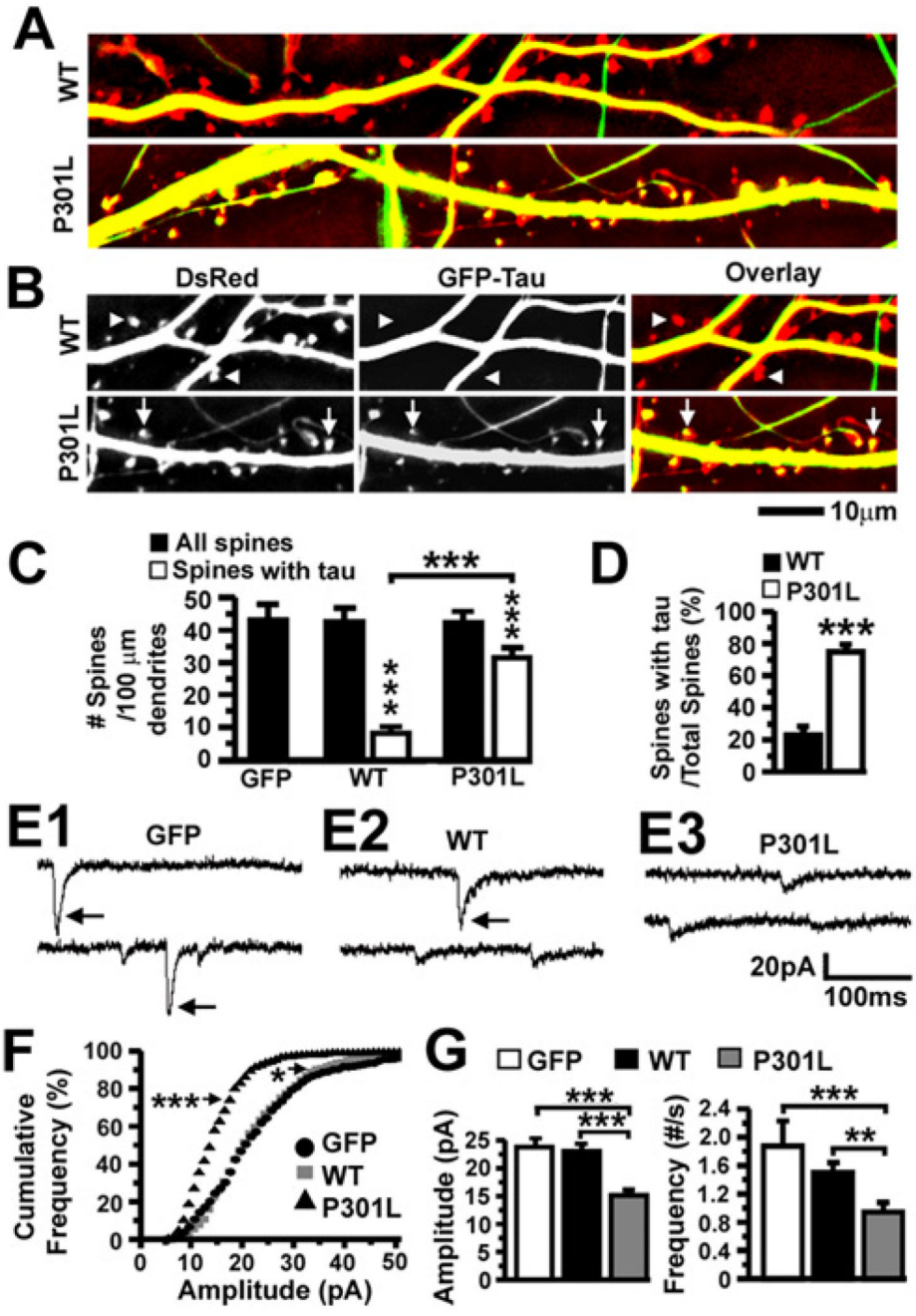

Figure 4. Effects of the FTDP-17-linked P301L mutation on tau accumulation in dendritic spines and excitatory synaptic transmission in transfected rat neurons

(A) Overlaid images of living dissociated rat hippocampal neurons (21–28 DIV) co-expressing DsRed and GFP-tagged htau proteins. (B) Cropped images from (A) including DsRed, GFP and overlaid images. Triangles denote dendritic spines devoid of WT htau and arrows denote spines containing P301L htau. See also Figure S2 for unprocessed raw images of cultured rat neurons co-transfected with DsRed and GFP-WT htau or GFP-P301L htau. (C) Quantification of total spines and htau-containing spines in neurons expressing GFP or co-expressing DsRed and GFP-tagged htau. There was more htau in the dendritic spines of neurons expressing P301L htau. n = 27 (GFP), 26 (WT) and 25 (P301L) neurons per group.

(D) A higher percentage of spines contained htau in neurons expressing P301L htau. (E) Representative mEPSCs in neurons expressing GFP (E1), GFP-tagged WT htau (E2) and GFP-tagged P301L htau (E3). Large mEPSCs occurred frequently in neurons expressing GFP or WT htau, but rarely in neurons expressing P301L htau. (F) Cumulative frequency distributions of mEPSC amplitudes of the neurons in (E). There were markedly more small mEPSCs in neurons expressing P301L htau than those expressing GFP. There was also a slight, but significant, decrease in the proportion of large events in neurons expressing WT htau. (Bin size = 1 pA) (G) Mean mEPSC amplitudes and frequencies of the neurons in (E). Neurons expressing P301L htau exhibited smaller and fewer mEPSCs. n = 14 (GFP), 14 (WT) and 16 (P301L) neurons per group. ANOVA followed by Bonferroni (C) or Fisher's PLSD (G) post-hoc analysis, t-test (D), Kolmogorov-Smirnov (F), *$p < 0.05$, **$p < 0.01$, ***$p < 0.001$.

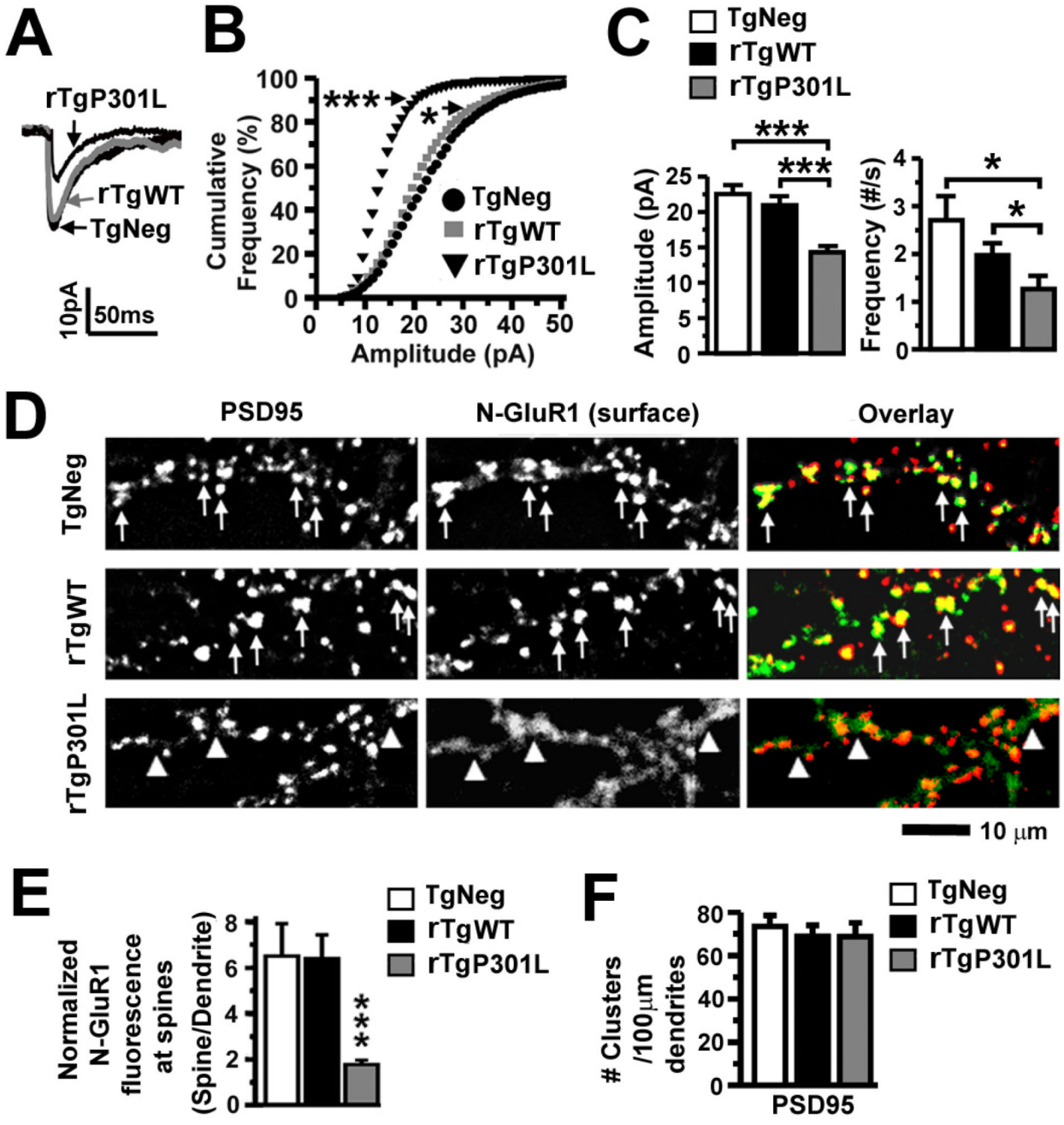

Figure 5. Excitatory synaptic transmission and surface AMPA receptors in rTgP301L and rTgWT neurons

(A) Representative averaged mEPSCs. (B) Cumulative frequency distribution of mEPSC amplitudes. There was a marked shift toward smaller amplitudes in rTgP301L neurons, and a slight shift toward smaller amplitudes in rTgWT neurons. (Bin size = 1 pA) (C) Mean mEPSC amplitudes and firing frequencies of the neurons in (A). rTgP301L neurons exhibited smaller and fewer mEPSCs. n = 15 (TgNeg), 15 (rTgWT) and 14 (rTgP301L) neurons per group. (D) PSD95 and surface AMPAR immunoreactivity. PSD95 (red) detected using a monoclonal antibody and surface AMPARs (green) detected using a polyclonal antibody against the N-terminus of GluR1 (N-GluR1) co-localized in TgNeg and

rTgWT neurons, but rarely in rTgP301L neurons. (E) Quantification of spine N-GluR1 immunoreactivity co-localizing with PSD95 immunoreactivity, normalized to N-GluR1 immunoreactivity on adjacent dendritic shafts. n = 10 neurons per group. (F) Density of dendritic spines labeled with a PSD95 antibody. There were no differences in the density of PSD95 immunoreactive clusters along the dendrites. n = 10 neurons per group. Kolmogorov-Smirnov (B), ANOVA followed by Fisher's PLSD post-hoc analysis (C, E, F), *$p < 0.05$, ***$p < 0.001$.

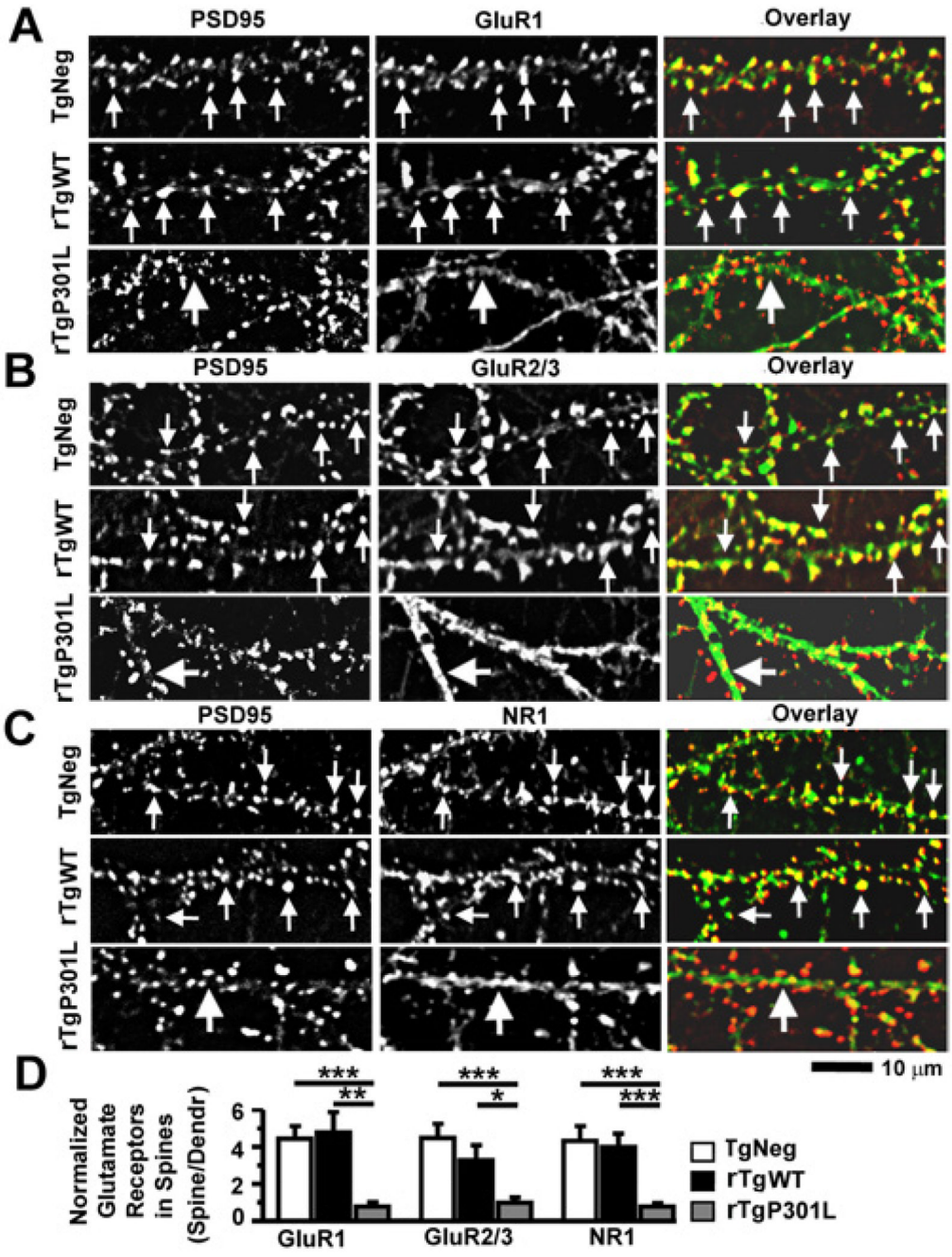

Figure 6. The P301L htau mutation disrupts clustering of GluR1, GluR2/3 and NR1 receptors at dendritic spines in cultured mouse neurons

(A) The PSD95 protein (*left column*) and the C-terminus of GluR1 subunits (*middle; overlay*, *right*) were co-stained with a mouse monoclonal antibody (red) and rabbit polyclonal antibody (green), respectively. Neurons (21–28 DIV) were cultured from TgNeg, rTgWT and rTgP301L mice (*from top to bottom*). Note that both surface and intracellular receptors were detected as all primary antibodies were added after the fixation and permeabilization of neurons. (B) Co-staining of PSD95 and GluR2/3 subunits (detected by an antibody that recognizes the C-termini of both GluR2 and GluR3). (C). Co-staining of PSD95 and NR1 (a mandatory subunit for functional NMDARs). (D) Quantification of spine

GluR1, GluR2/3 and NR1 immunoreactivity identified by co-localization with PSD95 immunoreactivity, normalized to GluR1, GluR2/3 and NR1 immunoreactivity on adjacent dendritic shafts, respectively. In all images, small arrows denote glutamate receptor clusters that co-localize with PSD95 clusters whereas large arrows denote diffuse staining of glutamate receptors in dendritic shafts. n = 10 neurons per group. ANOVA followed by Fisher's PLSD post-hoc analysis (D), *$p < 0.05$, **$p < 0.01$, ***$p < 0.001$.

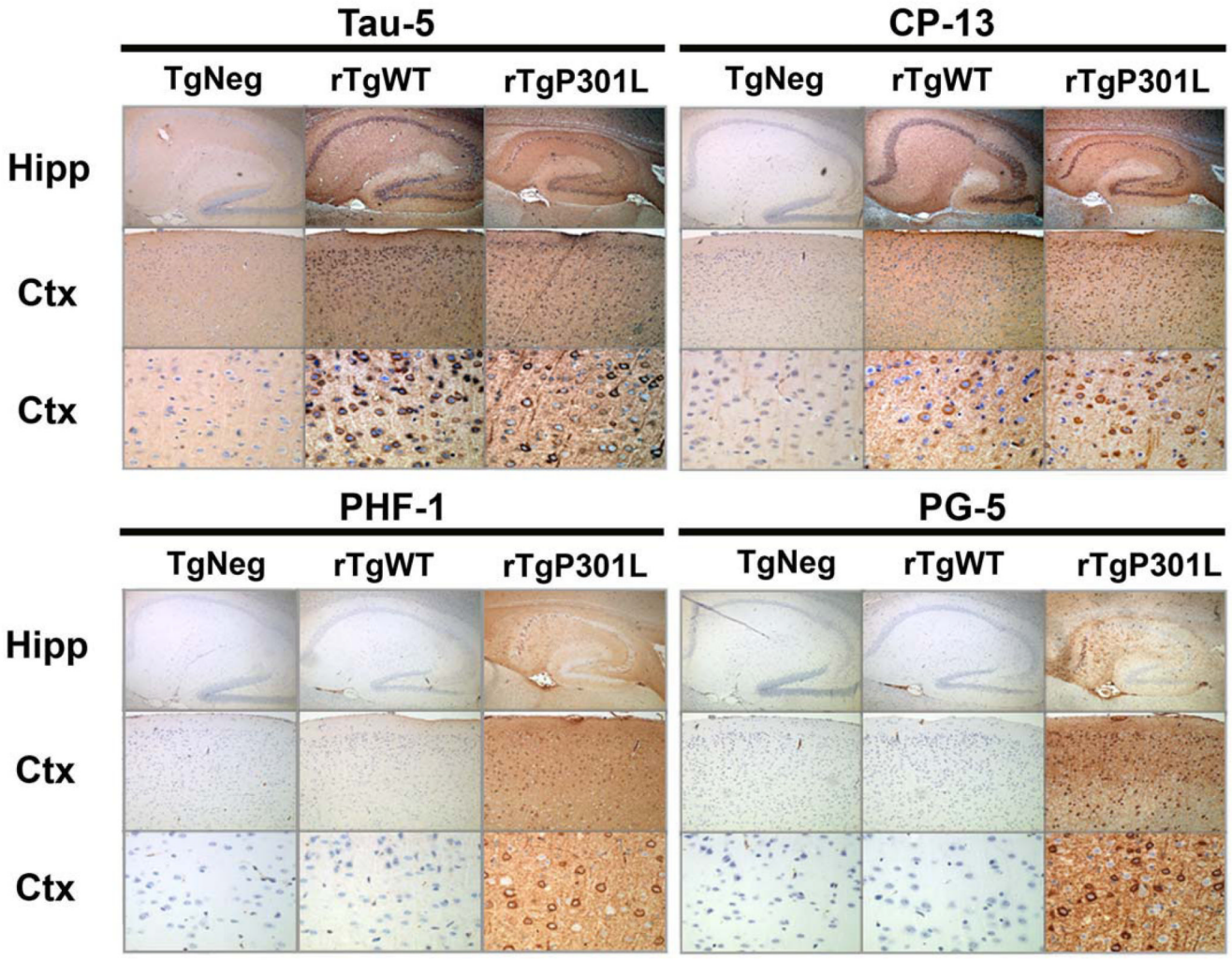

Figure 7. Pathological tau species do not accumulate in rTgWT mice

At 5 months of age (approximately when memory impairments begin, but before neuron loss), immunohistochemical studies revealed that cortical and hippocampal neurons in rTgWT mice were rarely immunoreactive for hyperphosphorylated tau species associated with disease. Detection of total tau (human and mouse) with the Tau-5 antibody in hippocampal and cortical neurons of rTgWT and rTgP301L mice. At 5 months, an immunoreactive signal for tau hyperphosphorylated at residue S202 (CP-13) was observed in the cell bodies of a small number of rTgWT hippocampal and cortical neurons. In contrast, CP-13 labeled-cell bodies and neurites were observed in a majority of rTgP301L hippocampal and cortical neurons. Strikingly, positive immunoreactive labeling for tau hyperphosphorylated at S409 (PG-5) and S396/S404 (PHF-1) was observed in hippocampal and cortical cell bodies and neurites of 5 month-old rTgP301L, but not rTgWT, mice. Nuclei were stained with DAPI. For each antibody panel, magnification was x5 (top row), x10 (middle row) and x40 (bottom row). Hipp, hippocampus; Ctx, cortex.

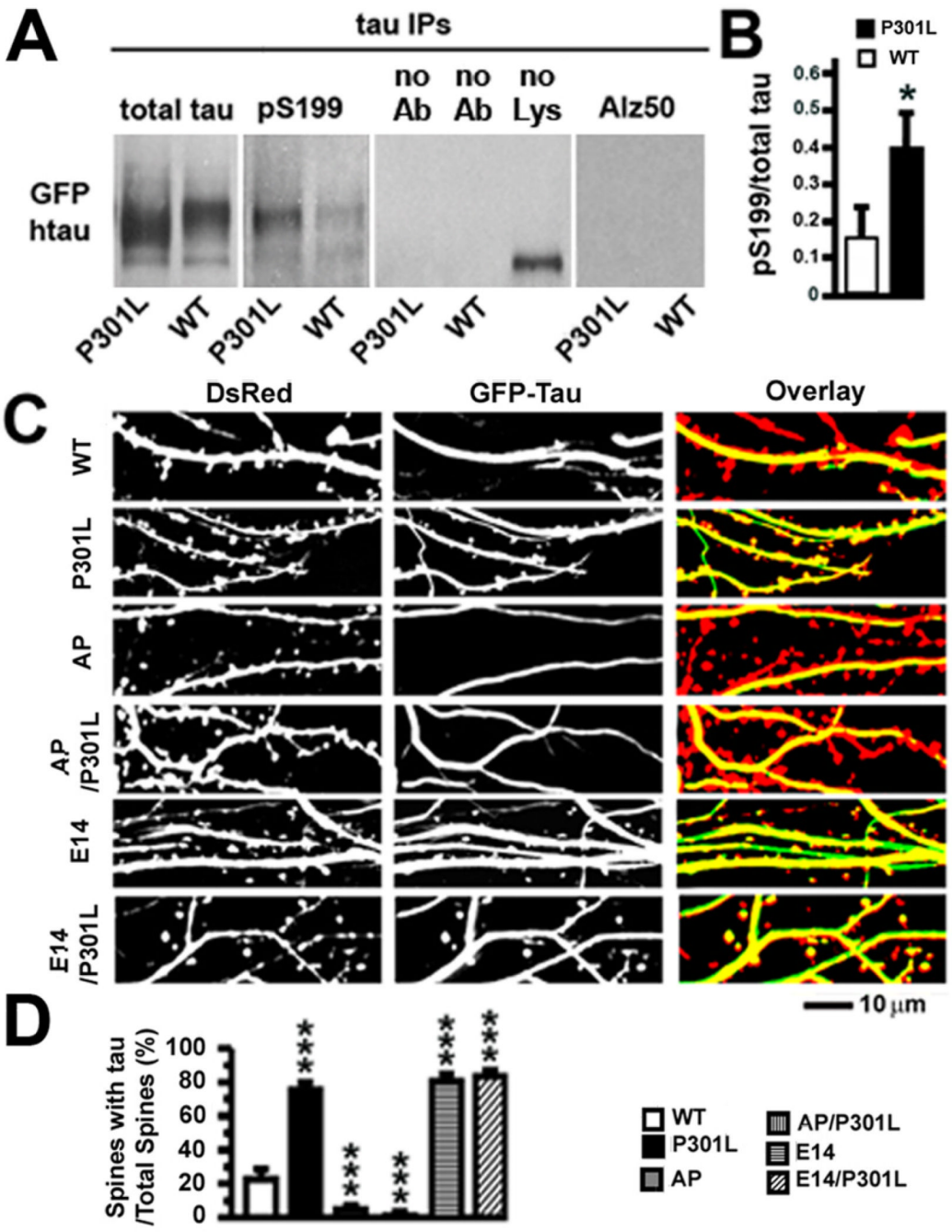

Figure 8. Hyperphosphorylation of P301L htau and effects of proline-directed phosphorylation on tau accumulation in dendritic spines of transfected rat hippocampal neurons

(A) Levels of phosphorylated htau in rat neurons expressing WT or P301L htau. Expression of total htau and phosphorylated S199 (pS199) htau proteins after immunoprecipitation of total htau with the Tau-13 antibody from 21–28 DIV primary rat hippocampal neurons expressing WT or P301L htau. Changes in tau conformation and phosphorylation states associated with late tau pathology were also examined with the Alz-50 antibody. In the middle panel, omission of the Tau-13 antibody (no Ab) or tissue lysate (no Lys) revealed no specific immunoblot signal for total htau. (B) There was more pS199, normalized to total tau, in the P301L htau-expressing neurons. n = 3 sample preparations. (C) Images of living

rat neurons co-expressing DsRed and six different GFP-tagged htau proteins (WT, P301L, AP, AP/P301L, E14 or E14/P301L). In neurons expressing WT, AP and AP/301L htau most DsRed-labeled spines were devoid of htau. In neurons expressing P301L, E14 and E14/P301L htau most spines contained htau. (D) Quantification of total spines and htau-containing spines in neurons co-expressing DsRed and GFP-tagged htau. A higher percentage of spines contained htau in neurons expressing P301L, E14 and E14/P301L htau (compared to WT htau), and a lower percentage of spines contained htau in neurons expressing AP and AP/P301L (compared to WT htau). n = 25–28 neurons per group. t-test (B), ANOVA followed by Bonferroni post-hoc analysis (D), *$p < 0.05$, ***$p < 0.001$.

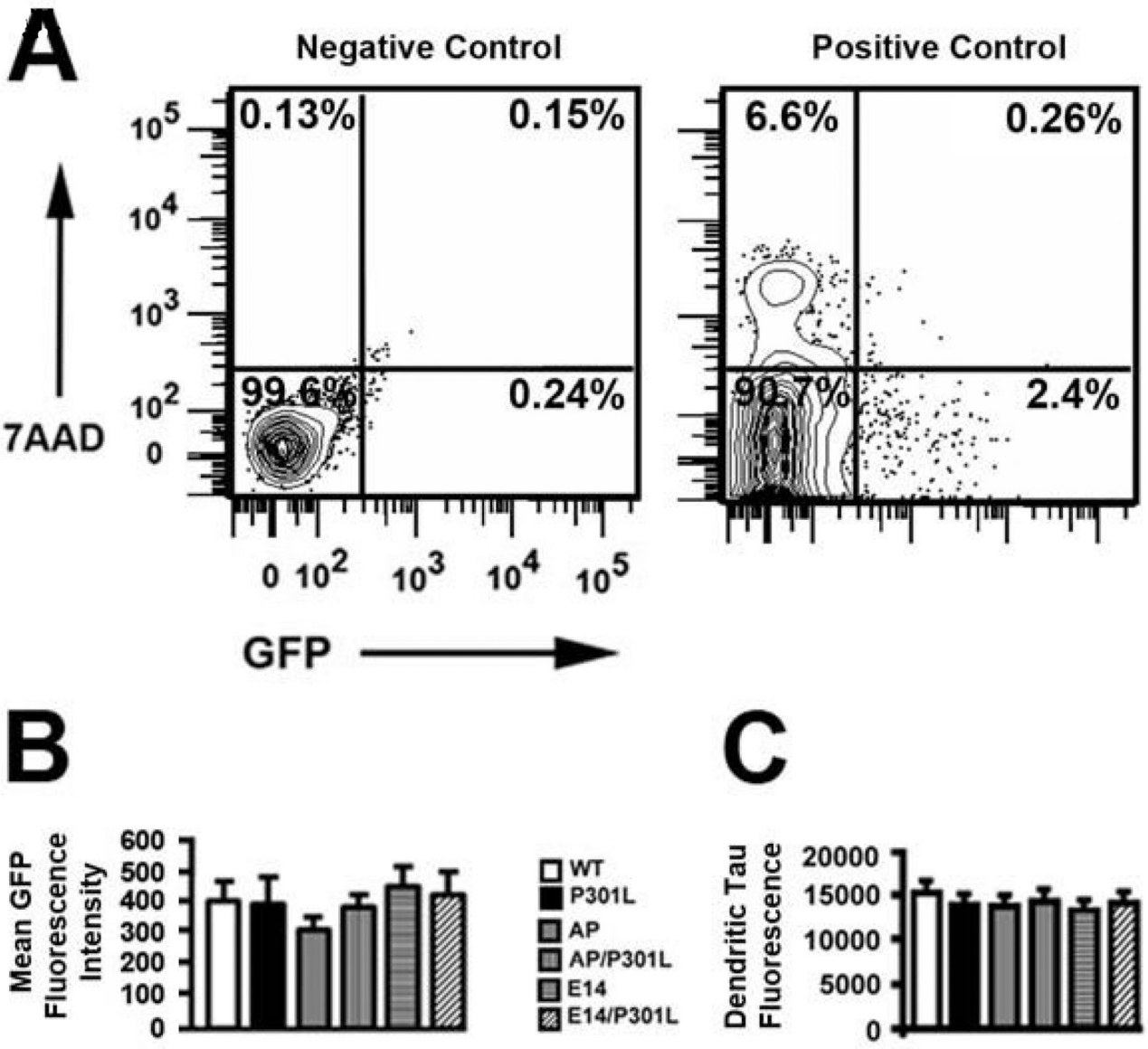

Figure 9. Quantitative measurement of GFP-htau expression levels in transfected rat hippocampal neurons

(A) Flow cytometry was used to measure GFP fluorescence intensity levels in hippocampal neurons transfected with WT and mutant GFP-htau. Untransfected hippocampal neurons served as a negative control (left panel, representative dot blot analysis) and neurons transfected with GFP alone were the positive control (right panel, representative dot blot analysis). The readout of GFP fluorescence in the right panel was used to determine the uniform gating parameters for counting GFP-positive events. Numbers in each quadrant are the percentage of cells in the respective quadrant. GFP-positive events are in the lower right quadrant. Dead neurons are in the upper left quadrant, as identified by increased fluorescence intensity of the DNA marker 7-aminoactinomycin D (7-AAD). Cellular debris is in the lower left and upper right quadrants.(B)Flow cytometry demonstrated that mean GFP fluorescence intensity did not differ significantly between different populations of hippocampal neurons transfected with GFP-htau constructs. n = 50,000 events sampled for each GFP-htau construct (10,000 events/GFP-htau construct × 5 different preparations). (C)

Fluorescent pixel intensity of GFP-tagged htau constructs in dendritic shafts. n = 19 neurons per group.

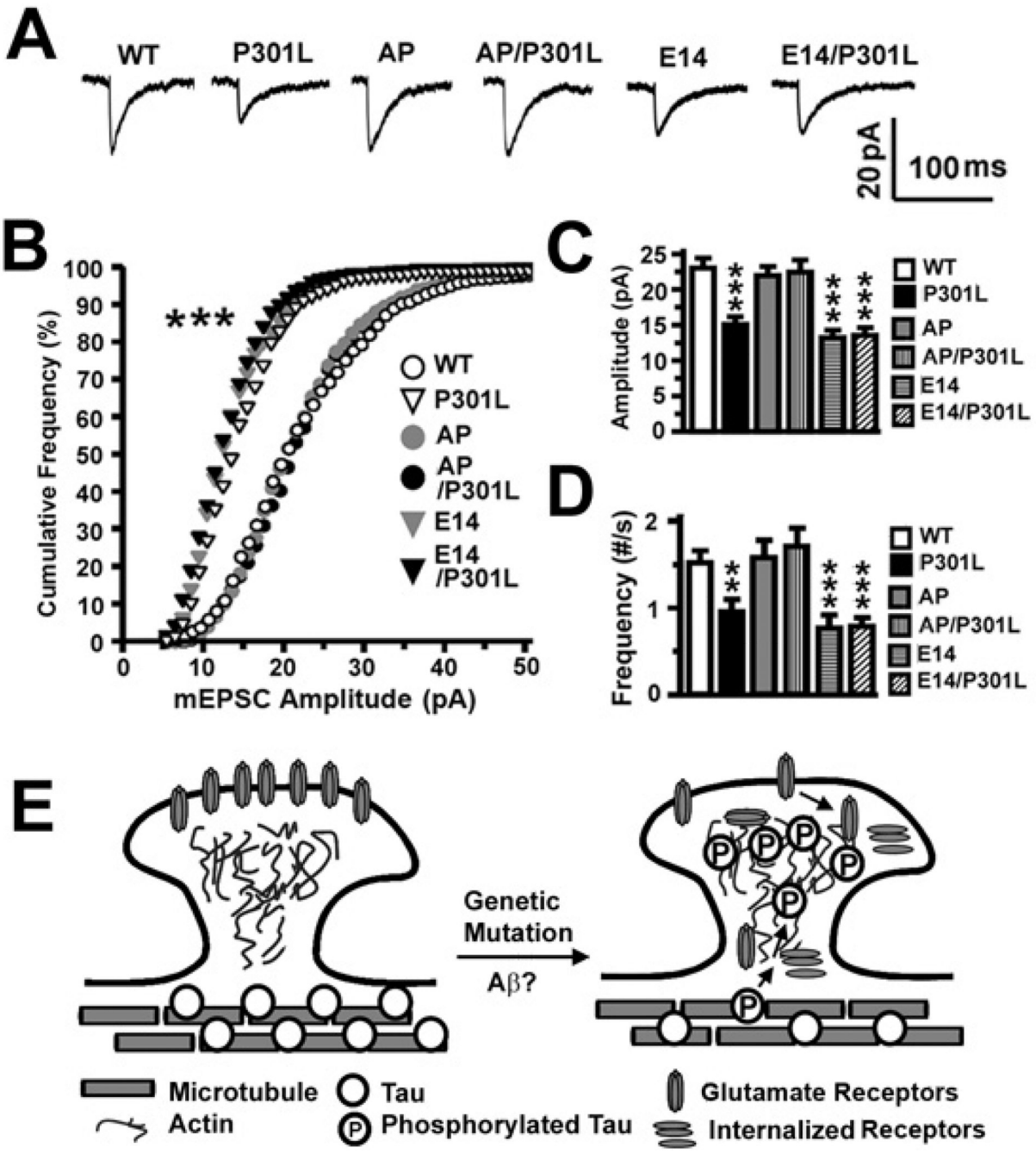

Figure 10. Effects of proline-directed phosphorylation of tau on excitatory synaptic transmission in transfected rat hippocampal neurons and a hypothetical model of tau-mediated synaptic dysfunction preceding neurodegeneration

(A) Representative averaged mEPSCs. (B) The cumulative frequency distribution of mEPSC amplitudes of neurons in (A). There was a shift toward smaller amplitudes in neurons expressing P301L, E14 and E14/P301L htau. (C) Mean mEPSC amplitudes and (D) frequencies of the neurons in (A). Neurons expressing P301L, E14 and E14/P301L htau exhibited smaller and fewer mEPSCs. n = 14 (WT), 16 (P301L), 15 (AP), 15 (AP/P301L), 15 (E14) and 15 (E14/P301L) neurons per group. (E) A diagram describing the hypothetical cellular processes underlying how hyperphosphorylated tau impairs excitatory synaptic

transmission through a loss of functional surface glutamate receptors. Since Aβ and genetic mutations in tau induce hyperphosphorylation of tau, we hypothesize that, following tau hyperphosphorylation, tau dissociates from the microtubules and is aberrantly targeted to dendritic spines, possibly through an actin-based process. Once mislocalized to the spines, tau impairs glutamatergic synaptic transmission by reducing the number of functional AMPA and NMDA receptors on the surface of the neuronal membrane through impaired anchoring of the glutamate receptors to the PSD complex, decreased exocytosis or increased endocytosis of the receptors. ANOVA followed by Fisher's PLSD post-hoc analysis (C, D), Kolmogorov-Smirnov (B), $^{**}p < 0.01$, $^{***}p < 0.001$.